1 # Reactions of Carbonyl Oxide with Aldehydes: Accurate Electronic
2 # Structure Methods, Kinetic Insights, and Atmospheric Implications

3 Chaolu Xie[1] Bo Long*[1,2]

4 [1] College of Physics and Mechatronic Engineering, Guizhou Minzu University, Guiyang 550025, China.

5 [2] College of Materials Science and Engineering, Guizhou Minzu University, Guiyang 550025, China

6 *Correspondence to*: Bo Long (wwwltcommon@sina.com)

7 **Abstract:** Carbonyl oxide (CH_2OO) is paramount in atmospheric oxidation chemistry, yet quantitative kinetics data for its

8 bimolecular reactions are very limited and even unknown. Here we establish a computational framework to obtain quantitative

9 kinetics from small to large reaction systems. For CH_2OO + HCHO, we develop electronic structure methods to reach

10 CCSDTQ/CBS accuracy for its activation enthalpies at 0 K. For CH_2OO + aldehydes (RCHO; R = CH_3-C_5H_{11}, CH_2F, CHF_2,

11 CF_3), we introduce two strategies that recover CCSDTQ/CBS-quality activation enthalpies at 0 K. A dual-level strategy has

12 been used to calculate their kinetics. The calculated rate constants show excellent agreement with available experimental data

13 for CH_2OO + RCHO (R = CH_3–C_3H_7), which validates the designed computational framework. We find that fluorination leads

14 to exceptional rate enhancement, with reactions of CHF_2CHO and CF_3CHO exceeding 10^{-10} cm^3 molecule^{-1} s^{-1} over 200–320

15 K, approaching the collision limit. We also find that fluorination-driven reactivity enhancement originates predominantly from

16 lower-level electronic effects than that of post-CCSD(T). Incorporation of the kinetics into a global chemical transport model

17 uncovers previously unrecognized atmospheric impacts, with CH_2OO + HCHO reducing nighttime CH_2OO and gas-phase

18 sulfate concentrations by 25.3% in Antarctica and 12.2% over Canada, respectively. The present findings address a long-term

19 challenge in how to obtain quantitative kinetics for large molecular systems, where post-CCSD(T) calculations are prohibitive

20 and provide new insights into the chemical transformation of CH_2OO and fluorinated aldehydes in the atmosphere.

21

---

*Corresponding author, E-mail: wwwltcommon@sina.com (Bo Long)

1 Introduction

Aldehydes are a major class of oxygenated volatile organic compounds (OVOCs) that substantially influence atmospheric oxidative capacity, secondary organic aerosol (SOA) formation, and air quality (Lary and Shallcross, 2000; Liu et al., 2022; Zhao et al., 2024; Li et al., 2024; Mellouki et al., 2015; Bao et al., 2025; Zhang et al., 2012; Bari and Kindzierski, 2018; Edwards et al., 2014; Yang et al., 2018). They originate from both direct emissions—including biomass and fossil-fuel combustion, biogenic sources, and vehicle exhaust—and secondary production via VOC oxidation (Zhao et al., 2024; Knote et al., 2014; Parrish et al., 2012; Chen et al., 2014; Luecken et al., 2012; Grosjean et al., 1983). Their atmospheric removal is governed primarily by photolysis and OH reactions during daytime, whereas fluorinated aldehydes exhibit notably reduced OH reactivity (Wenger, 2006; Jiménez et al., 2007; Atkinson and Pitts, 1978; Lily et al., 2021; Sellevåg et al., 2005; Scollard et al., 1993; Thévenet et al., 2000; D'anna et al., 2001). NO_3 reactions constitute a nighttime sink but proceed extremely slow, highlighting the need to identify alternative nocturnal loss pathways (Cabañas et al., 2001; Bossmeyer et al., 2006; Papagni et al., 2000).

Stabilized Criegee intermediates (sCIs), key intermediate species of O_3-initiated alkene ozonolysis (Criegee, 1975; Criegee and Wenner, 1949), play critical roles in atmospheric oxidation and SOA formation (Khan et al., 2018; Novelli et al., 2014; Percival et al., 2013; Chhantyal-Pun et al., 2020) and react rapidly with acids (Cabezas and Endo, 2019; Chung et al., 2019; Peltola et al., 2020; Foreman et al., 2016; Raghunath et al., 2017), amides (Wei et al., 2022; Long et al., 2025), and SO_2 (Berndt et al., 2014; Boy et al., 2013; Manonmani et al., 2023; Kukui et al., 2021). Accurate kinetics for their bimolecular reactions are therefore essential for constraining their atmospheric fate.

45 **Table 1.** Rate constants of $CH_2OO + HCHO$ by previous investigation at different temperatures and pressures.

Reaction	P (Torr)	T (K)	k(T) (cm^3 molecule^{-1} s^{-1})	Ref.
Exp.	56	296	$(4.11 \pm 0.25) \times 10^{-12}$	(Luo et al., 2023)
	78	275	$(4.84 \pm 0.41) \times 10^{-12}$	(Enders et al., 2024)
		295	$(3.50 \pm 0.35) \times 10^{-12}$	
Theory	10	213	3.28×10^{-9}	(Zhang et al., 2023)
	202	230	1.29×10^{-9}	
	406	259	3.52×10^{-10}	
	760	296	5.51×10^{-10}	
		295	5.71×10^{-10}	
		296	6.52×10^{-11}	(Long et al., 2021)
		275	1.11×10^{-10}	
		295	6.68×10^{-11}	
		296	3.01×10^{-11}	This work
		275	5.62×10^{-11}	
		295	3.10×10^{-11}	

46   Despite numerous studies on CH_2OO + aldehydes, important gaps remain (Tables 1–3): for $CH_2OO + HCHO$, theoretical

47 and experimental rate constants differ by an order of magnitude (Luo et al., 2023; Enders et al., 2024; Long et al., 2021; Zhang

48 et al., 2023); prior work on $CH_2OO + CH_3CHO/C_2H_5CHO/C_3H_7CHO$ relied primarily on CCSD(T) despite evidence that

49 higher-level excitations are required (Taatjes et al., 2012; Elsamra et al., 2016; Stone et al., 2014; Berndt et al., 2015; Jiang et

50 al., 2024; Kaipara and Rajakumar, 2018; Liu et al., 2020; Liu et al., 2023; Cornwell et al., 2023; Debnath and Rajakumar,

51 2024); and key effects such as anharmonicity, torsional anharmonicity, and recrossing were generally neglected (Luo et al.,

52 2023; Enders et al., 2024; Kaipara and Rajakumar, 2018; Debnath and Rajakumar, 2024; Jalan et al., 2013).

53

54

55

56

57

58

59 **Table 2.** Rate constants of $CH_2OO + CH_3CHO$ by previous investigation at different temperatures and pressures.

Reaction	P (Torr)	T (K)	$k(T)$ (cm^3 $molecule^{-1}$ s^{-1})	Ref.
Exp.	4	293	$(9.50 \pm 0.70) \times 10^{-13}$	(Taatjes et al., 2012)
	25	298	$(1.20 \pm 0.20) \times 10^{-12}$	(Elsamra et al., 2016)
		340	$(8.00 \pm 1.10) \times 10^{-13}$	
	4	298	$(1.10 \pm 0.10) \times 10^{-12}$	
	50		$(1.30 \pm 0.20) \times 10^{-12}$	
	25	295	$(1.48 \pm 0.04) \times 10^{-12}$	(Stone et al., 2014)
	760	297	$(1.70 \pm 0.50) \times 10^{-12}$	(Berndt et al., 2015)
	78	275	$(2.37 \pm 0.21) \times 10^{-12}$	(Enders et al., 2024)
		295	$(1.61 \pm 0.14) \times 10^{-12}$	
	50	280	$(2.57 \pm 0.46) \times 10^{-12}$	(Jiang et al., 2024)
		298	$(2.13 \pm 0.38) \times 10^{-12}$	
	5.5	298	$(1.73 \pm 0.32) \times 10^{-12}$	
	10		$(2.08 \pm 0.38) \times 10^{-12}$	
	30		$(2.10 \pm 0.38) \times 10^{-12}$	
	50		$(2.13 \pm 0.38) \times 10^{-12}$	
	100		$(2.16 \pm 0.38) \times 10^{-12}$	
	80	275	$(10.20 \pm 0.80) \times 10^{-13}$	(Cornwell et al., 2023)
		295	$(8.00 \pm 0.70) \times 10^{-13}$	
Theory	760	275	4.63×10^{-12}	This work
		280	4.02×10^{-12}	
		293	2.83×10^{-12}	
		295	2.69×10^{-12}	
		297	2.56×10^{-12}	
		298	2.50×10^{-12}	

60   Moreover, no kinetic data exist for reactions with larger or fluorinated aldehydes, including pentanal, hexanal, CH_2FCHO,

61 CHF_2CHO, and CF_3CHO. Owing to the substantial uncertainties in computed atmospheric reaction kinetics, atmospheric

62 models have traditionally relied on rate constants estimated from empirical structure–reactivity relationships rather than from

63 first-principles calculations (Jenkin et al., 2018). This reliance underscores the need for computational frameworks capable of

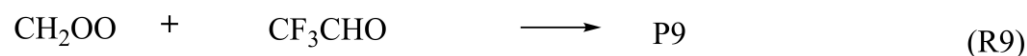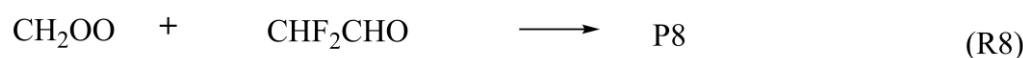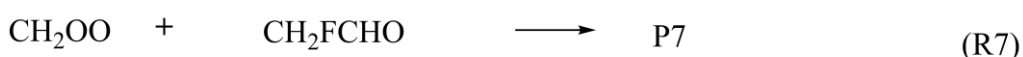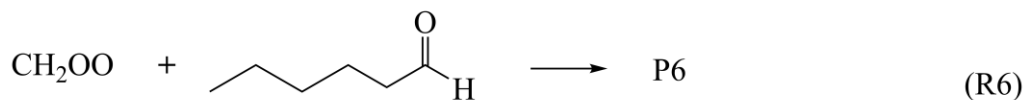64 delivering quantitatively reliable kinetics across chemically diverse atmospheric systems.

65

66   **Table 3.** Rate constants of $CH_2OO + RCHO$ (R = C_2H_5/C_3H_7) by previous investigation at different temperatures and pressures.

Reaction		P	T	$k(T)$ (cm³ molecule⁻¹ s⁻¹)	Ref.
C_2H_5CHO	Exp.	50 Torr	283 K	$(3.55 \pm 0.50) \times 10^{-12}$	(Liu et al., 2020)
			298 K	$(3.12 \pm 0.44) \times 10^{-12}$	
		5 Torr	298 K	$(2.39 \pm 0.22) \times 10^{-12}$	
		5.2 Torr		$(2.52 \pm 0.24) \times 10^{-12}$	
		10 Torr		$(3.07 \pm 0.20) \times 10^{-12}$	
		25 Torr		$(2.12 \pm 0.19) \times 10^{-12}$	
		75 Torr		$(3.30 \pm 0.20) \times 10^{-12}$	
		100 Torr		$(3.08 \pm 0.19) \times 10^{-12}$	
		150 Torr		$(3.18 \pm 0.19) \times 10^{-12}$	
		200 Torr		$(3.19 \pm 0.21) \times 10^{-12}$	
		78 Torr	275 K	$(4.35 \pm 0.38) \times 10^{-12}$	(Enders et al., 2024)
			295 K	$(3.29 \pm 0.29) \times 10^{-12}$	
	Theory	HPL	283 K	2.29×10^{-12}	(Kaipara and Rajakumar, 2018)
			298 K	1.51×10^{-12}	
			275 K	2.92×10^{-12}	
			295 K	1.63×10^{-12}	
			283 K	4.49×10^{-12}	This work
			298 K	3.11×10^{-12}	
			275 K	5.57×10^{-12}	
			295 K	3.33×10^{-12}	
C_3H_7CHO	Exp.	50 Torr	253 K	$(4.20 \pm 0.10) \times 10^{-12}$	(Debnath and Rajakumar, 2024)
			268 K	$(3.61 \pm 0.10) \times 10^{-12}$	
			283 K	$(2.99 \pm 0.22) \times 10^{-12}$	
			298 K	$(2.63 \pm 0.14) \times 10^{-12}$	
	Theory	HPL	253 K	8.83×10^{-12}	This work
			268 K	5.30×10^{-12}	
			283 K	3.38×10^{-12}	
			298 K	2.27×10^{-12}	

67   Here, we investigate CH_2OO reactions with nine aldehydes (RCHO; R = H, CH_3, C_2H_5, C_3H_7, C_4H_9, C_5H_{11}, CH_2F, CHF_2,

68   CF_3) to obtain quantitative rate constants and to establish a general high-accuracy computational protocol applicable from

69   small benchmark systems to large atmospheric molecules. For the prototypical $CH_2OO + HCHO$ reaction, we develop the

70   GMM(Q).L4 composite scheme that approaches full-CI accuracy, and for the broader reaction suite we devise a scalable

71   strategy capable of delivering near–full-CI activation energies. Dual-level strategy calculations accounting for all major

72   anharmonic and dynamical effects yield benchmark-quality rate constants, which are subsequently implemented in GEOS-

73   Chem to quantify their atmospheric impacts. This work provides a broadly extensible computational framework and

74   significantly advances the understanding of CH_2OO–aldehyde chemistry.

$$CH_2OO + HCHO \longrightarrow HCOOH + HCHO \quad (R1)$$

$$CH_2OO + CH_3CHO \longrightarrow P2b \quad (R2)$$

$$CH_2OO + \quad \longrightarrow P3 \quad (R3)$$

$$CH_2OO + \quad \longrightarrow P4 \quad (R4)$$

$$CH_2OO + \quad \longrightarrow P5 \quad (R5)$$

$$CH_2OO + \quad \longrightarrow P6 \quad (R6)$$

$$CH_2OO + CH_2FCHO \longrightarrow P7 \quad (R7)$$

$$CH_2OO + CHF_2CHO \longrightarrow P8 \quad (R8)$$

$$CH_2OO + CF_3CHO \longrightarrow P9 \quad (R9)$$

75
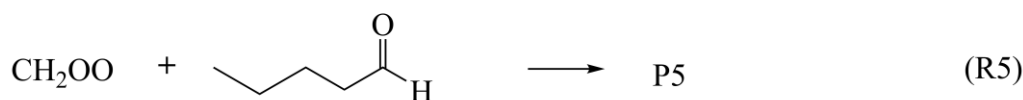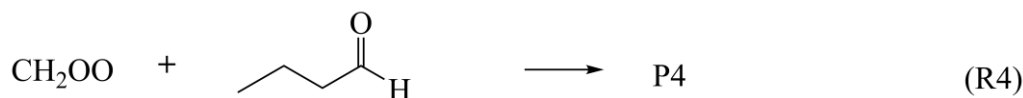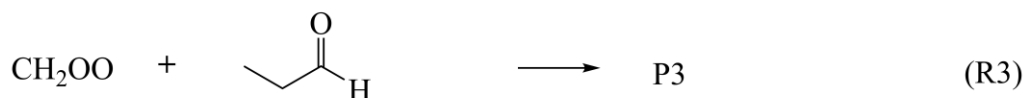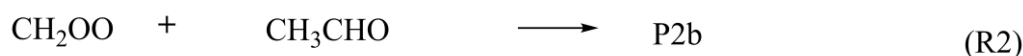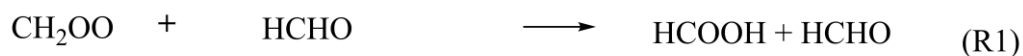
76   **Scheme 1.** Reactions of CH_2OO with aldehydes

2 Computational methods and strategies

2.1 Electronic structure best estimates for the CH₂OO + HCHO reaction

Accurate electronic-structure data are essential for quantitative kinetics. All geometries and harmonic frequencies were optimized at the CCSD(T)-F12a/cc-pVTZ-F12 level (Adler et al., 2007; Knizia et al., 2009; Bischoff et al., 2009). To approach the full-CI limit for single-point energies, we developed a composite protocol, GMMQ.L4, which effectively reproduces CCSDTQ/CBS quality:

$$E_{\text{GMMQ.L4}} = E_{\text{MW2-F12.L}} + \Delta E_{\text{T-(T)}} + \Delta E_{\text{(Q)-T}} + \Delta E_{\text{Q-(Q)}} \quad (1)$$

Here, $E_{\text{MW2-F12.L}}$ is obtained from the previously validated MW2-F12.L scheme. $\Delta E_{\text{T-(T)}}$ (CCSDT–CCSD(T)) and $\Delta E_{\text{(Q)-T}}$ (CCSDT(Q)–CCSDT) are extrapolated to the CBS limit (cc-pVDZ → cc-pVTZ and cc-pVDZ → VTZ(d)) using

$$\Delta E_{\text{L}} = \Delta E_{\text{CBS}} + \frac{A}{L^3} \qquad (2)$$

with $L = 2,3$.

The final correction, $\Delta E_{\text{Q-(Q)}}$, is evaluated at the CCSDTQ–CCSDT(Q) level using the VDZ(NP) basis set. VTZ(d) employs H(s) and heavy-atom(spd), while VDZ(NP) uses H(s) and heavy-atom(sp) functions (Chan and Radom, 2015).

Coupled-cluster theory converges systematically toward Full configuration interaction (Full-CI), but the steep scaling necessitates truncation. Previous studies have established rapid basis-set convergence for both CCSDT(Q)–CCSDT and CCSDT–CCSD(T) (Long et al., 2021; Long et al., 2019; Xia et al., 2025). Consistently, the CCSDTQ–CCSDT(Q) contribution in our system is only 0.096 kcal mol⁻¹, indicating that excitations beyond quadruples contribute <0.10 kcal mol⁻¹ in Table S1. Thus, GMMQ.L4//CCSD(T)-F12a/cc-pVTZ-F12 serves as the benchmark level in our dual-level kinetics framework.

We further compared GMMQ.L4 with the W3X-L composite method (Chan and Radom, 2015) for reaction R1. The deviation of 0.24 kcal mol⁻¹ demonstrates that W3X-L is insufficient to obtain quantitatively accurate barrier heights for this system. Additionally, CCSD(T)-F12 convergence was verified by comparing W2X energies computed with cc-pVTZ-F12 and cc-pVDZ-F12 geometries; the difference of only 0.04 kcal mol⁻¹ confirms near-CBS performance of CCSD(T)-F12 for structural and vibrational data (See Table 4).

101 **Table 4.** Calculated enthalpies of activation at 0 K ($\Delta H_0^{\ddagger}$ in kcal/mol, relative to the bimolecular reactants) and unsigned
102 deviation (MUD) (in kcal/mol).

Methods	$\Delta H_0^{\ddagger}$	
	TS1	UD
GMMQ.L4//CCSD(T)-F12a/cc-pVTZ-F12	−4.97	0.00
BE1//CCSD(T)-F12a/cc-pVTZ-F12	−4.97	0.00
BE2//CCSD(T)-F12a/cc-pVTZ-F12	−4.97	0.00
M11-L/MG3S	−5.16	0.19
W3X-L//CCSD(T)-F12a/cc-pVTZ-F12	−5.22	0.24
MW2-F12.L//CCSD(T)-F12a/cc-pVTZ-F12	−5.41	0.44
W2X//DF-CCSD(T)-F12a/jun-cc-pVDZ	−5.60	0.63
W2X//CCSD(T)-F12a/cc-pVTZ-F12	−5.62	0.64
W2X//CCSD(T)-F12a/cc-pVDZ-F12	−5.66	0.68
W2X//DF-CCSD(T)-F12b/VDZ(d)	−5.66	0.68
W2X//DF-CCSD(T)-F12a/cc-pVDZ	−5.72	0.74
W2X//DF-CCSD(T)-F12b/VDZ(NP)	−6.19	1.22

103 **2.2 Electronic structure best estimates for R2-R9**

104   **Geometrical optimization and frequency calculations.** Reliable optimized geometries and harmonic frequencies are

105 essential for obtaining quantitative 0 K activation enthalpies. For reaction R1, we verified that CCSD(T)-F12a/cc-pVDZ-F12

106 delivers results essentially identical to CCSD(T)-F12a/cc-pVTZ-F12, allowing us to employ the lower-cost cc-pVDZ-F12

107 basis for reaction R2. However, for larger CH_2OO + aldehyde systems, CCSD(T)-F12a/cc-pVDZ-F12 remains computationally

108 prohibitive. To overcome this limitation, we systematically benchmarked density-fitted F12 coupled-cluster methods (DF-

109 CCSD(T)-F12b) (Győrffy and Werner, 2018) across a range of compact basis sets (Table 4). Remarkably, DF-CCSD(T)-

110 F12b/jun-cc-pVDZ (Parker et al., 2014) and DF-CCSD(T)-F12b/VDZ(d) exhibit exceptionally small mean unsigned

111 deviations of only 0.03 and 0.04 kcal mol⁻¹, respectively, relative to the Best Estimate for W2X reference (Table S2).This

112 identifies a new, computationally efficient F12 protocol capable of retaining sub-0.05 kcal mol⁻¹ accuracy for CH_2OO–

113 aldehyde reactions, representing a key methodological advance enabling routine treatment of larger Criegee intermediate–

114 carbonyl systems. Accordingly, we employed DF-CCSD(T)-F12b/jun-cc-pVDZ for R3–R5 and R7–R8, and DF-CCSD(T)-

115 F12b/VDZ(d) for R3–R6 to obtain geometries and vibrational frequencies with near-CBS accuracy at greatly reduced cost.

116 ***Single point energy calculations.*** To further reduce the cost of CCSDTQ/CBS-quality calculations, we developed a new

117 composite scheme, denoted BE1, which achieves near-GMMQ.L4 accuracy. The BE1 single-point energy is defined as

118
$$E_{BE1} = E_{W2X} + \Delta E_{(Q)-(T)} + \Delta E_{SC1} \qquad (3)$$

119 where $\Delta E_{(Q)-(T)}$ is the CCSDT(Q) – CCSD(T) correction evaluated with the VDZ(NP) basis set for reactions R1–R8.

120 The term ΔE_{SC1} introduces a structure-specific correction and is given by

121
$$\Delta E_{SC1} = E_{GMMQ.L4}^{TS1} - E_{W2X}^{TS1} - [E_{CCSDT(Q)/VDZ(NP)}^{TS1} - E_{CCSD(T)/VDZ(NP)}^{TS1}] \qquad (4)$$

122 This formulation anchors the composite energy to a single high-level reference transition state (TS1), ensuring the

123 transferability of the correction across the reaction series. The value of ΔE_{SC1} is 0.04 kcal/mol.

124 For comparison, we also employed our previously reported strategy, BE2 (Sun et al., 2024), which augments the W2X

125 energy with a constant post-CCSD(T) correction:

126
$$E_{BE2} = E_{W2X} + \Delta E_{SC2} \qquad (5)$$

127 where ΔE_{SC2} is the GMMQ.L4 − W2X difference for TS1 (0.64 kcal mol^{-1} in Table 4).

128 Both BE1 and BE2 offer computationally inexpensive routes to emulate CCSDTQ/CBS performance by incorporating

129 systematic, physically motivated corrections. In the present work, the BE1 protocol served as the high-level (HL) energy in

130 our dual-level kinetics strategy, with the underlying structures obtained from

131 • BE1//CCSD(T)-F12a/cc-pVDZ-F12 for R2,

132 • BE1//DF-CCSD(T)-F12b/jun-cc-pVDZ for R3–R5 and R7–R8, and

133 • BE1//DF-CCSD(T)-F12b/VDZ(d) for R6.

134 This composite strategy enables sub-kcal mol^{-1} accuracy at a fraction of the cost of full GMMQ.L4 or CCSDTQ/CBS

135 calculations.

136 **2.3. Electronic structure density functional methods**

137 To enable efficient direct kinetics calculations for the full aldehyde series, we systematically evaluated a range of density

138 functional methods against the BE1 benchmark. Among all tested functionals, M11-L (Peverati and Truhlar, 2012)/MG3S

(Lynch et al., 2003) exhibits the best performance, yielding a remarkably small mean unsigned deviation (MUD) of 0.32 kcal

mol^{-1} across reactions R1–R8 (Figure 1). This accuracy—well within sub-kcal mol^{-1} agreement with the BE1 high-level

reference—identifies M11-L/MG3S as a reliable and computationally economical low-level (LL) method for the dual-level

kinetics framework. Accordingly, M11-L/MG3S was used for all direct kinetics calculations involving CH_2OO + aldehyde

reactions. Standard vibrational scaling factors were applied as listed in Table S3.
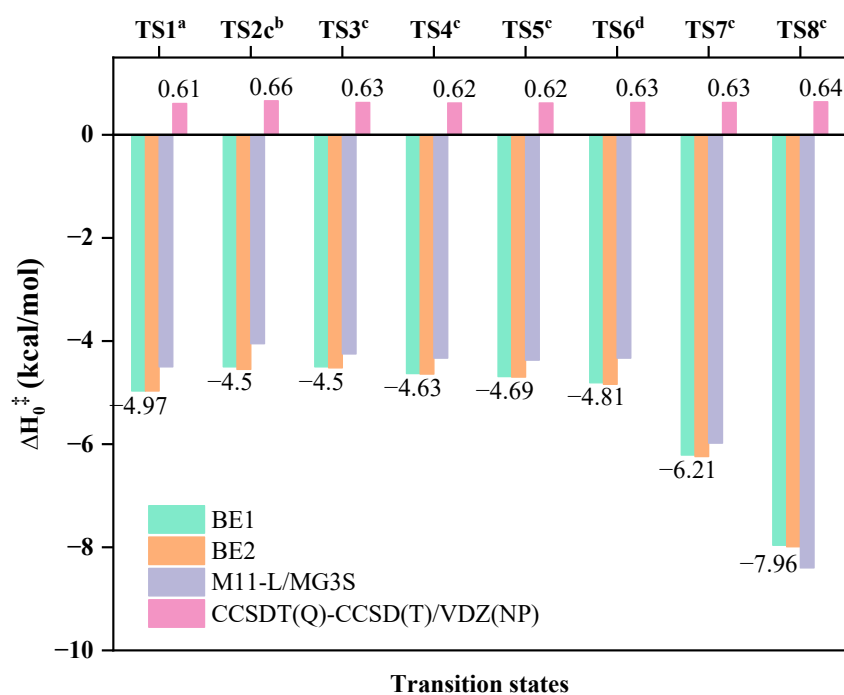
Figure 1. Best estimate for reaction R1-R8 at different level.

[a]The best estimate results by BE1//CCSD(T)-F12a/cc-pVTZ-F12 in the CH_2OO + HCHO reaction.

[b]The best estimate results by BE1//CCSD(T)-F12a/cc-pVDZ-F12 in the CH_2OO + CH_3CHO reaction.

[c]The best estimate results by BE1//DF-CCSD(T)-F12b/jun-cc-pVDZ in the CH_2OO + XCHO $(X=C_2H_5/C_3H_7/C_4H_9/CH_2F/CHF_2)$ reaction.

[d]The best estimate results by BE1//DF-CCSD(T)-F12b/VDZ(d) in the CH_2OO + $C_5H_{11}CHO$ reaction.

Previous studies have suggested that standard scaling factors may be unsuitable for certain transition states, we explicitly

investigated the impact of anharmonicity. Using the method described by Long et al. (Long et al., 2023), we calculated specific

scaling factors by (See Tables S4 and S5). However, we found that anharmonicity corrections to the zero-point energy (ZPE)

were negligible. Consequently, standard scaling factors are employed throughout this work. Full methodological details are

155   provided in the Supporting Information.

156   **2.4. Kinetics Methods**

157   ***High-pressure limited rate constants for R2-R6.*** Dual-level strategy (Long et al., 2019; Sun et al., 2024; Long et al.,

158   2016) was employed, in which high-level (HL) conventional transition state theory (TST) provides the baseline rate constants,

159   whereas canonical variational transition state theory with small-curvature tunneling (CVT/SCT) at the low-level (LL) supplies

160   kinetic corrections. The high-pressure-limit rate constants were obtained according to eq 5:

$$k = k_{HL}^{TST}(T)\kappa_{LL}(T)\Gamma_{LL}(T)F_{fwd}^{MS-T,LL}(T) \tag{5}$$

162   where k_{HL}^{TST} is the rate constants calculated at HL. $\kappa_{LL}(T)$ and $\Gamma_{LL}(T)$ is tunneling and recrossing transmission coefficients

163   calculated at the LL level. $F_{fwd}^{MS-T,LL}(T)$ is referred to multi-structural anharmonic factor calculated by eqn (6) at the M11-

164   L/MG3S level

$$F_{fwd}^{MS-T,LL} = \frac{F_{TS}^{MS-T}}{F_{R}^{MS-T}} \tag{6}$$

166   ***High-pressure limited rate constants for R1 and R7-R9.*** The rate constants of R1 and R7-R9 were calculated by

167   simultaneously considering both the loose transition state between reactants and the van der Waals complex, and the tight TS

168   between reactants and products. The rate constant for the loose TS (k_{loose}) was calculated using variable-reaction-coordinate

169   variational transition-state theory (VRC-VTST) (Georgievskii and Klippenstein, 2003; Zheng et al., 2008; Bao et al., 2016b)

170   with 500 configurations for Monte Carlo sampling. A single-faceted dividing surface was constructed with two pivot points,

171   following procedures validated in previous work (Long et al., 2021). One pivot point was placed along a vector at a distance

172   *d* from the center of mass (COM) of CH_2OO, oriented perpendicular to the CH_2OO plane, while the other was placed similarly

173   with respect to $CH_2F/CHF_2/CF_3CHO$. The pivot distance was set to *d*=0.05 Å. The reaction coordinate *s* was defined as the

174   separation between the two pivot points, ranging from 3.5 to 10 Å for R7, 3.9 to 10 Å for R8, 4.4 to 10 Å for R9 with increments

175   of 0.1 Å. The rate constant for the tight TS (k_{tight}) was calculated by using dual-level strategy presented above. The overall

176   rate constant was then obtained using the steady-state approximation (Garrett and Truhlar, 1982; Zhang et al., 2020; Long et

177   al., 2024) in equation (7).

178
$$k = \frac{k_{\text{loose}}k_{\text{tight}}}{k_{\text{loose}}+k_{\text{tigh}t}}$$
(7)

179   ***Pressure-dependent rate constant.*** Master equation method with Rice−Ramsperger−Kassel−Marcus theory (ME/RRKM)

180   (Kenneth A. Holbrook, 1996; Fernández-Ramos et al., 2006; Georgievskii et al., 2013; Klippenstein, 2003) was used to

181   calculate pressure dependence of rate constants for the reactions of CH_2OO with HCHO and CH_3CHO. The calculation utilized

182   parameters from W3X-L//CCSD(T)-F12a/cc-pVTZ-F12 for reaction R1 and W2X//DF-CCSD(T)-F12b/jun-cc-pVDZ for

183   reaction R2. Both reactions were modeled with N_2 as the bath gas, employing Lennard-Jones parameters from Table S6 and

184   an average energy transfer parameter of $<\Delta E>_{\text{down}}$ = 200 cm^{-1}. Within this framework, the pressure effect was approximated

185   as the quotient of the high-pressure limit and a pressure ratio. This ratio is defined as the value at 7.5×10^3 Torr relative to its

186   value at different pressures. We further inspection the simplification of reaction R2 in Scheme 2. The kinetic results for

187   Schemes 2a and 2b demonstrate remarkable robustness, with the simplification introducing no statistically significant

188   perturbations to the calculated rate constants.

189
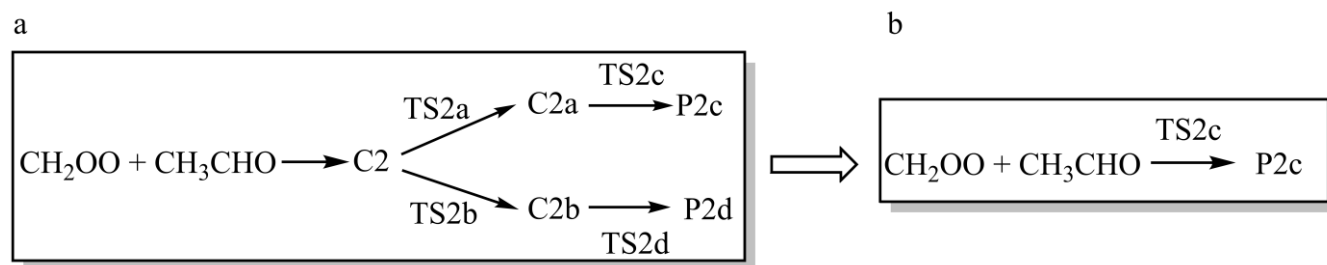
190   **Scheme 2**. The reaction mechanism for the CH_2OO + CH_3CHO reaction.

191   **2.5. Atmospheric modeling**

192   We performed two atmospheric simulations included reaction R1 and R2 to investigate the significance of these reactions

193   by observing the change of concentration globally in GEOS-Chem. This included: (1) a "base" model using default setting (2)

194   a "update1" model adding a new sink of HCHO in the base model, (3) a "update2" model adding a new sink of CH_3CHO in

195   the base model. These models include the meteorological data observations assimilated from the NASA Modern-Era

196   Retrospective Analysis for Research and Applications (MERRA-2) (Gelaro et al., 2017) and Emissions data from the default

197   Harmonized Emission Component (HEMCO) (Lin et al., 2021). For anthropogenic emissions, we used the Community

198   Emissions Data System (CEDS) (Hoesly et al., 2018). For biogenic emissions, we used offline VOC emissions computed from

199   the Model of Emissions of Gases and Aerosols from Nature (MEGAN) (Guenther et al., 2012). The simulation was carried out

200   with $2° \times 2.5°$ horizontal resolution at 47 vertical layers. The annual changes displayed are obtained from simulations that

201   employed meteorological data from February 1, 2018, to January 31, 2019, following a six-month model spin-up.

202   **2.6. Software.**

203   Density functional calculations were performed by using the Gaussian 16 (Frisch et al., 2016). The coupled cluster

204   calculations were performed by using the Molpro 2019 (Werner, 2019) and MRCC codes (Kállay et al., 2020). Multi-structural

205   anharmonic calculations were performed in MSTor codes (Zheng et al., 2012). Rate constants were calculated using the

206   Polyrate 2017-C (Zheng et al., 2017b), Gaussrate 2017-B codes (Zheng et al., 2017a), and KiSThlP 2021 (Canneaux et al.,

207   2014). The master equation calculations were performed by utilizing the TUMME program (Zhang et al., 2022). Atmospheric

208   modeling was performed by using GEOS-Chem 14.4.2 (Bey et al., 2001, (http://www.geos-chem.org, last access: 4 November

209   2025).

210   **3. RESULTS AND DISSCUSSION**

211   The enthalpy of activation at 0 K ($\Delta H_0^{\ddagger}$) is referred to the relative energies with zero-point energy between transition states

212   and reactants.

213   **3.1 The electronic structure of CH₂OO + HCHO**

214   The reaction mechanism examined here is consistent with that established in earlier studies (Luo et al., 2023; Long et al.,

215   2021; Jalan et al., 2013; Wang et al., 2022). The relative enthalpy profile for the CH_2OO + HCHO reaction is depicted in Figure

216   2, and the key data are summarized in Table 4. Notably, the activation enthalpy at 0 K obtained at the GMMQ.L4//CCSD(T)-

217   F12a/cc-pVTZ-F12 level (-4.97 kcal mol⁻¹) differs from that predicted by W3X-L//CCSD(T)-F12a/cc-pVTZ-F12 (-5.21 kcal

218   mol⁻¹ in Table 4) and deviates even more substantially from the RCCSD(T)-F12a/VTZ-F12//B3LYP/MG3S value (-6.30 kcal

219   mol⁻¹) (Jalan et al., 2013). These differences demonstrate the strong sensitivity of $\Delta H_0^{\ddagger}$ to the underlying electronic-structure

220   treatment, thereby directly influencing predicted rate constants.

221
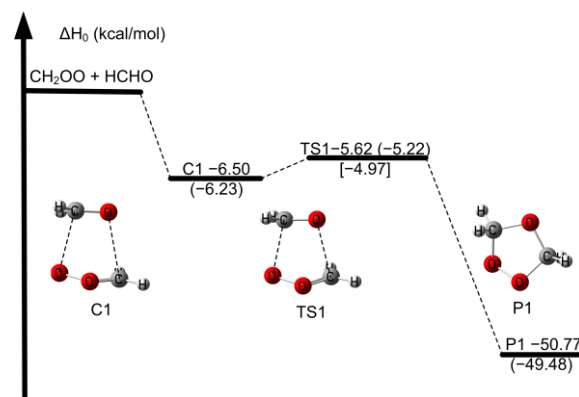
Figure 2. The relative enthalpies at 0 K for the reaction of $CH_2OO + HCHO$. Values are given for all species as calculated by W2X//CCSD(T)-F12a/cc-pVTZ-F12, and in parentheses and bracket, values are given for the transition state TS1 as calculated by W3X-L//CCSD(T)-F12a/cc-pVTZ-F12 and GMMQ.L4//CCSD(T)-F12a/cc-pVTZ-F12.

Previous studies have shown that post-CCSD(T) correlation is essential for quantitative barriers in Criegee chemistry (Long et al., 2021; Long et al., 2016; Xia et al., 2022). For TS1, the unsigned deviation between GMMQ.L4 and MW2-F12.L is 0.40 kcal mol^{-1}—slightly different with the ~0.50 kcal mol^{-1} benchmark established for post-CCSD(T) effects (Long et al., 2021)—reaffirming the need for high-level correlation to achieve quantitative accuracy. We further find that the post-CCSD(T) contribution through CCSDT(Q), quantified by the W3X-L − W2X difference, is 0.44 kcal mol^{-1}, in excellent agreement with the 0.40 kcal mol^{-1} value. This concordance highlights the robustness of W3X-L in capturing post-CCSD(T) contributions (Table 4). The remaining 0.24 kcal mol^{-1} discrepancy between GMMQ.L4 and W3X-L primarily reflects differences between the MW2-F12.L and W2X components of TS1 (Table S7). The 0.21 kcal mol^{-1} deviation between MW2-F12.L and W2X further illustrates that larger basis sets are required for fully quantitative predictions.

This present work provides a rigorously benchmarked assessment of $\Delta H_0^{\ddagger}$ for the $CH_2OO + HCHO$ reaction, explicitly quantifying post-CCSD(T) contributions and revealing their decisive role in achieving sub-kcal mol^{-1} accuracy. The systematic comparison among GMMQ.L4, MW2-F12.L, and W3X-L underscores the reliability of our calculated results.

3.2. The electronic structure of $CH_2OO + CH_3CHO$

We aim to demonstrate the feasibility of simplifying the reaction mechanism of larger aldehydes with CH_2OO in Scheme

239 2. A partial reaction mechanism $CH_2OO + CH_3CHO$ has been reported in our previous work (Wang et al., 2022). We first

240 consider the seven-membered ring precreation complex C2 formation in Figure 3, which is consistent with our previous results

241 (Wang et al., 2022). However, due to two distinct orientations of the methyl group in CH_3CHO toward CH_2OO, there are two

242 rotation transition states TS2a and TS2b connecting C2 to the five-membered ring complexes C2a and C2b, respectively.

243 Therefore, the process is only the transformation of complex in the reaction processes. Then, C2a and C2b undergo the

244 corresponding transition state TS2c and TS2d responsible for the formation of P2a and P2b. The mechanism was depicted in

245 Scheme 2a. However, the enthalpies of activation at 0 K for TS2a and TS2b are lower than those of TS2c and TS2d by 0.64

246 kcal/mol and 0.37 kcal/mol at W3X-L//CCSD(T)-F12a/cc-pVDZ-F12 in Figure 3, respectively. Therefore, TS2a and TS2b

247 could be neglected from energetic point of view. We will also discuss it from the kinetics point of view.
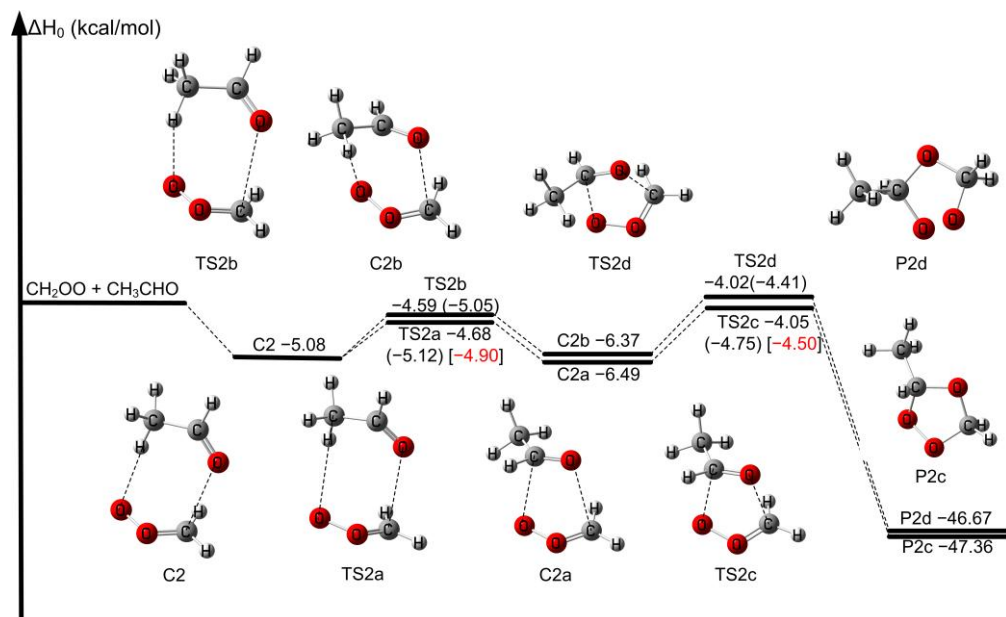
Figure 3. The relative enthalpies at 0 K for the reaction of $CH_2OO + CH_3CHO$. Values are given for all species as calculated by M11-L/MG3S, and in parentheses and bracket, values are given for the transition states as calculated by W3X-L//CCSD(T)-F12a/cc-pVDZ-F12 and BE1//CCSD(T)-F12a/cc-pVDZ-F12.

252 The five-membered ring complexes C2a and C2b can interconvert via $TS2_{ISO}$ with C=O bond rotation, which lies 2.51

253 kcal mol^{-1} above C2a at the M11-L/MG3S level (Figure S4), similar to the reaction between CH_2OO and FCHO (Xia et al.,

254 2024). For aldehydes with longer chains, the corresponding isomerization transition states of the five-membered ring

255 complexes (Figures S5–S6) exhibit similarly low barriers, indicating facile interconversion. Consequently, the complex

256 mechanism can be effectively reduced to the straightforward reaction pathway b depicted in Scheme 2. Accordingly, the

257 mechanism for CH_2OO with larger aldehydes was simplified to consider only the lowest-energy pathway corrected by torsional

258 anharmonicity in kinetics calculations.

259   The $\Delta H_0^\ddagger$ for TS2c is -4.50 kcal mol^{-1} at the BE1//CCSD(T)-F12a/cc-pVDZ-F12 level (See Table S8), which is 0.8 kcal

260 mol^{-1} higher than the result reported by Jalan et al. at the RCCSD(T)-F12a/VTZ-F12//B3LYP/MG3S level and 0.19 kcal mol^{-1}

261 higher than that of Wang et al at the WMS//M11-L/MG3S level (Wang et al., 2022; Jalan et al., 2013). BE1 and BE2 for TS2c

262 agree well with each other in Figure 1 and Table S8, not only demonstrating the reliability of the computational protocol, but

263 also capturing the essential physical origin underlying the quantitative description of $\Delta H_0^\ddagger$. The M11-L/MG3S has been chosen

264 for direct dynamics calculations due to the MUD of 0.81 kcal mol^{-1} in Table S8.

265   The validity of the DF-CCSD(T)-F12/jun-cc-pVDZ and DF-CCSD(T)-F12b/VDZ(d) methods was also confirmed for

266 reaction R2. As shown in Table S8, these methods yielded mean unsigned deviations (MUD) of 0.05 and 0.02 kcal mol^{-1},

267 respectively, relative to the CCSD(T)-F12a/cc-pVDZ-F12 benchmark.

268 **3.3. Electronic structure of CH_2OO + RCHO (R = C_2H_5/C_3H_7/C_4H_9/C_5H_{11})**

269   The complexity of reactions R3–R6 increases with reactant system size owing to the presence of multiple conformers of

270 both reactants and transition states (Table S9). Specifically, two conformers were identified for C_2H_5CHO, four for C_3H_7CHO,

271 twelve for C_4H_9CHO, and thirty-five for $C_5H_{11}CHO$, arising from C–C bond rotations. In contrast, conformational diversity is

272 even more pronounced for the transition states, with three conformers for TS3, eighteen for TS4, twenty-four for TS5, and

273 seventy-nine for TS6, primarily due to internal C=O and C-C bond rotations.

274   As the carbon chain prolongs, the change in $\Delta H_0^\ddagger$ for R1-R6 is not obvious, but it presents a trend. We find a slight

275 decrease in $\Delta H_0^\ddagger$ with the elongation of carbon chain for R2-R6 with the exception of R1. The $\Delta H_0^\ddagger$ calculated by best

276 estimate are -4.50, -4.50, -4.63, 4.69, and -4.81 kcal mol^{-1} for R2-R6 (See Figure 1 and Table S10), which are about 3 kcal

277 mol^{-1} below the reaction of the corresponding reactants with HO_2 (Gao et al., 2024; Long et al., 2022; Ding and Long, 2022).

278 Moreover, the influence of carbon chain length on enthalpy of activation for R2-R6 is analogue to the reaction of HO_2 and

279 aldehydes (Gao et al., 2024). Also, BE1 and BE2 for TS2c–TS6 (Figure 1 and Table S10) exhibit excellent mutual consistency.

280   This behavior can be attributed to the nearly invariant $(CCSDT(Q) - CCSD(T))/VDZ(NP)$ term (~0.6 kcal mol^{-1}) among

281   these transition states, demonstrating that the post-CCSD(T) contributions are almost uniform across this reaction series. These

282   observations provide compelling evidence that both alkyl substitution and carbon-chain elongation negligibly modulate the

283   magnitude of post-CCSD(T) corrections, implying that such higher-order correlation effects are intrinsically insensitive to

284   substituent-induced electronic and conformational changes.

285   **3.4. Electronic structure of CH$_2$OO + RCHO (R = CH$_2$F/CHF$_2$/CF$_3$)**

286   The electronic structure information was depicted in Figure 1, S3, and Table S11. The activation enthalpies at 0 K decrease

287   significantly with the increasing number of fluorine substitutions in the methyl group of the aldehyde.

288   The $\Delta H_0^{\ddagger}$ for CH$_2$OO + CH$_2$FCHO (TS7) is -6.21 kcal mol^{-1} by our best estimate, which is 1.31 kcal mol^{-1} and 1.71

289   kcal mol^{-1} lower than the reaction R1 and R2, respectively. Consequently, reaction R7 is expected to exhibit a significantly

290   larger rate constant compared to the CH$_2$OO + HCHO/CH$_3$CHO reactions. This reduction in $\Delta H_0^{\ddagger}$ indicates that fluorine

291   substitution enhances the reactivity of the aldehyde toward CH$_2$OO, which is similar to HO$_2$ + CF$_3$CHO (Long et al., 2022).

292   For the reaction of CH$_2$OO + CHF$_2$CHO (R8), the $\Delta H_0^{\ddagger}$ is -7.96 kcal mol^{-1}, which is 1.75 kcal mol^{-1} lower than that of the

293   corresponding transition state, TS7. This value is close to that of CH$_2$OO + HCl (Foreman et al., 2016), which approaches the

294   bimolecular collision limit, suggesting that the reaction R8 through the tight transition state is not the rate-determining step.

295   Although fluorine substitution on the methyl group of the aldehyde leads to substantially enhanced reactivity toward CH$_2$OO,

296   the post-CCSD(T) contributions from the $(CCSDT(Q) - CCSD(T))/VDZ(NP)$ term (~0.6 kcal mol^{-1}) remain nearly identical

297   across the transition states as shown in Figure 1, revealing that the higher-order correlation effects are largely insensitive to

298   fluorination and establishing that the fluorination-driven reactivity enhancement originates primarily from lower-level

299   electronic effects than that of post-CCSD(T).

300   Given the demonstrated accuracy of the M11-L/MG3S method for reactions R7 and R8, this method was subsequently

301   applied to reaction R9, as depicted in Figure S3. Regarding CF$_3$CHO + CH$_2$OO (R9), the $\Delta H_0^{\ddagger}$ further decreases to -9.74

302   kcal/mol at M11-L/MG3S level. However, this value is slightly higher than the activation enthalpies observed for the universal

303   mechanism of Criegee intermediates reacting with amides (Long et al., 2025), which are significantly submerged below the

17

304 reactants by approximately 9 to 11 kcal/mol. This shows that this tight transition state is not the rate-determining step for

305 reaction R9.

306   We further compare the calculated $\Delta H_0^{\ddagger}$ of the CH$_2$OO + RCHO (R = CH$_2$F, CHF$_2$, CF$_3$) reactions with those of the

307 corresponding OH reactions. The $\Delta H_0^{\ddagger}$ for OH + CH$_2$FCHO is −1.15 kcal mol^{-1} at the CCSD(T)//M06-2X/aug-cc-pVTZ level,

308 which is 5.06 kcal mol^{-1} higher than that of R7. We also find that the $\Delta H_0^{\ddagger}$ for R8 by our best estimate is 8.19 kcal mol^{-1} lower

309 than that of OH + CHF$_2$CHO, calculated at the CCSD(T)/aug-cc-pVDZ//MP2(FC)/aug-cc-pVDZ level. The $\Delta H_0^{\ddagger}$ for R9

310 calculated by M11-L/MG3S is 11.94 kcal/mol lower than that of OH + CF$_3$CHO at QCISD(T)/6-311G(d,p) level (Chandra et

311 al., 2001). The present findings reveal that the much lower $\Delta H_0^{\ddagger}$ for R7-R9 leads to a much faster rate constant, indicating

312 that oxidation by CH$_2$OO contributes significantly to the atmospheric loss of fluorinated aldehydes relative to the OH-initiated

313 pathway from energetic point of view.

314 **3.5. Kinetics**

315 **3.5.1 Pressure-dependent rate constants.**

316   The pressure dependence of the rate constants for reactions R1 and R2 was evaluated using the ME/RRKM framework,

317 with the results summarized in Tables S12–S14. As shown in Table S12, reaction R1 exhibits no appreciable pressure

318 dependence over the conditions examined, indicating that pressure effects can be safely neglected for this channel. This

319 conclusion is fully consistent with the findings reported by Luo et al (Luo et al., 2023). For example, the falloff factor of 1.34

320 calculated for the CH$_2$OO + HCHO reaction at 298 K and 0.0316 bar (Table S12) confirms weak pressure dependence, a

321 finding consistent with the results of Luo et al (Luo et al., 2023). We observed that at 295 K and 78 Torr, the pressure-dependent

322 rate constant was 2.71 × 10^{-11} cm^3 molecule^{-1} s^{-1} in Table S12, which is 7.74 times higher than the reported value ((3.50 ±

323 0.35) × 10^{-12} cm^3 molecule^{-1} s^{-1}) in Table 1 (Enders et al., 2024).

324   We assessed the validity of the simplified pathway by contrasting the full mechanism (Scheme 2a) with the model

325 (Scheme 2b) from a kinetic perspective as listed in Tables S13 and S14. The pressure-dependent rate constants obtained from

326 both models exhibit negligible deviations, thereby validating the simplified scheme as a computationally efficient strategy for

327 larger aldehydes. The calculated pressure-dependent rate constant for reaction R2 is 1.84×10^{-12} cm^3 molecule^{-1} s^{-1} at 293 K

328 and 4 Torr in Table S13, in good agreement with the value of $(9.50 \pm 0.70) \times 10^{-13}$ cm^3 molecule^{-1} s^{-1} reported by Taatjes et al

329 (Taatjes et al., 2012). Our pressure-dependent rate constant at 298 K and 25 Torr corroborates the experimental value of (1.20

330 $\pm$ 0.20) $\times 10^{-12}$ cm^3 molecule^{-1} s^{-1} reported by Elsamra et al (1.65×10^{-12} cm^3 molecule^{-1} s^{-1} in Table S13) (Elsamra et al.,

331 2016). We found that the fall-off factor is only 1.36 (Table S13) for the reaction R2 at 298 K and 4 Torr, which also shown that

332 the rate constant of reaction R2 is negligibly pressure-dependent, which confirms the experimental results qualitatively (Enders

333 et al., 2024; Stone et al., 2014; Berndt et al., 2015; Jiang et al., 2024). In addition, there is experimental evidence that the

334 pressure effect is also insignificant for propionaldehyde and butyraldehyde (Liu et al., 2020; Debnath and Rajakumar, 2024).

335 **3.5.2 High pressure limit rate constants**

336 High-pressure limit rate constants for all reactions are summarized in Table 5, with additional details provided in Tables

337 S15–S23. The rate constants in the temperature range of 190–350 K were fitted using the four-parameter expression (Zheng

338 and Truhlar, 2012; Bao et al., 2016a):

$$k_\infty = A \left(\frac{T + T_0}{300}\right)^n \exp\left[-\frac{E(T + T_0)}{R(T^2 + T_0^2)}\right] \qquad (7)$$

340 Where R is the gas constant, T is temperature in K, the fitting parameters were listed in Table S24. The temperature dependence

341 of the Arrhenius activation energies was further calculated using the following expression:

$$E_a = -R\frac{d\ln k_\infty}{d(1/T)} \qquad (8)$$

Table 5. The high-pressure limiting rate constants ($\times$ 10^{-12} cm^3 molecule^{-1} s^{-1}) of the CH$_2$OO + RCHO (R = H/CH$_3$/C$_2$H$_5$/C$_3$H$_7$/C$_4$H$_9$/C$_5$H$_{12}$/CH$_2$F/CHF$_2$/CF$_3$) reaction

T/K	k_1	k_2	k_3	k_4	k_5	k_6	k_7	k_8	k_9
200	426	96	105	115	106	214	430	451	740
220	297	32.7	36.1	40.8	36	71.9	248	416	688
240	171	13.6	15	17.5	14.8	29.5	115	381	652
260	90.4	65.4	7.27	8.72	6.75	13.1	51.1	328	626
280	48.0	3.55	3.93	4.86	3.64	7.09	24	252	607
298	28.3	2.27	2.45	3.10	2.28	4.46	13.1	182	594
300	26.8	2.11	2.34	2.97	2.22	4.41	12.3	174	593
320	15.9	1.35	1.49	1.95	1.37	2.67	6.90	110	583
340	10.0	9.22	1.01	1.35	0.93	1.80	4.17	67.4	576

The reaction of CH₂OO + HCHO. As summarized in Table 1 and Figure 4, a long-standing order-of-magnitude discrepancy exists between previously reported experimental and theoretical rate constants for reaction R1. At 296 K, the rate constant obtained in this work is 3.01×10^{-11} cm^3 molecule^{-1} s^{-1} in Table 1, which is 7.31 times larger than the experimental value reported by Luo et al (Luo et al., 2023). but 1.83 and 2.17 times smaller than the theoretical predictions of Zhang et al. (Zhang et al., 2023) and Long et al. (Long et al., 2021), respectively. Although the present value does not fully reconcile the experimental and theoretical results, it substantially narrows the gap between the two, providing a quantitatively improved estimate for this key reaction.
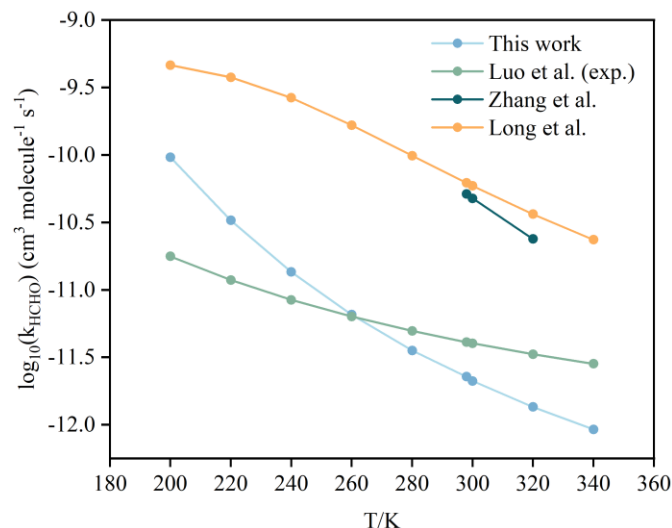
Figure 4. A comparison of reported rate constants for the CH$_2$OO + HCHO reaction from previous studies at different

361 temperatures and high-pressure limit.

362   Notably, the derived rate constant for R1 is approximately 8 times larger than that for the corresponding OH-initiated

363 reaction and more than two orders of magnitude larger than that for the HO_2-initiated pathway (Long et al., 2022; Sivakumaran

364 et al., 2003), highlighting the unexpectedly high reactivity of CH_2OO in this system. These findings underscore the need for

365 further high-precision experimental measurements and establish the present computational protocol as a robust framework for

366 resolving persistent discrepancies in atmospheric reaction kinetics.

367   ***The reaction of $CH_2OO + CH_3CHO$.*** To date, no theoretical kinetic studies have been reported for the $CH_2OO + CH_3CHO$

368 reaction in Table 2. The earliest experimental determination yielded a rate constant of $(9.50 \pm 0.25) \times 10^{-13}$ cm^3 molecule^{-1} s^{-1}

369 at 293 K and 4 Torr, as measured by Taatjes et al. (Taatjes et al., 2012), which is a factor of 2.9 smaller than the present

370 theoretical prediction in Table 2. At 298 K, the calculated rate constant for reaction R2 is 2.50×10^{-12} cm^3 molecule^{-1} s^{-1} in

371 Table 2, in excellent agreement with the experimental values reported by Elsamra et al. (Elsamra et al., 2016) and Jiang et al.

372 (Jiang et al., 2024) In addition, the value measured by Berndt et al. (Berndt et al., 2015) at 297 K, $(1.7 \pm 0.50) \times 10^{-12}$ cm^3

373 molecule^{-1} s^{-1}, is fully consistent with our calculated result of 2.56×10^{-12} cm^3 molecule^{-1} s^{-1} in Table 2. Overall, the rate

374 constants obtained in this work are in good agreement with the available experimental data (Elsamra et al., 2016; Stone et al.,

375 2014; Berndt et al., 2015; Jiang et al., 2024; Cornwell et al., 2023), providing the first reliable theoretical benchmark for the

376 kinetics of the $CH_2OO + CH_3CHO$ reaction. Notably, the rate constant for R2 is approximately 5.6 times smaller than that for

377 the corresponding OH-initiated reaction, yet nearly two orders of magnitude larger than that for the HO_2-initiated pathway,

378 highlighting the distinct and non-negligible role of CH_2OO in aldehyde oxidation chemistry (Long et al., 2022; Zhu et al.,

379 2008).

380   ***The reaction of $CH_2OO + RCHO$ (R=C_2H_5/C_3H_7/C_4H_9/C_5H_{11}).*** Rate constants for the reactions of CH_2OO with

381 C_2H_5CHO have been reported previously from both experimental and theoretical studies (See Table 3) (Enders et al., 2024;

382 Kaipara and Rajakumar, 2018; Liu et al., 2020), whereas the reaction with C_3H_7CHO has been examined only experimentally.

383 At 298 K, the calculated rate constant for $CH_2OO + C_2H_5CHO$ is 3.11×10^{-12} cm^3 molecule^{-1} s^{-1} (Table 3), in excellent

384 agreement with the experimental value reported by Liu et al (Liu et al., 2020).

385   For $CH_2OO + C_3H_7CHO$, the calculated rate constant of 3.10×10^{-12} cm^3 molecule^{-1} s^{-1} (Table 3) closely reproduces the

386 experimental value of $(2.63 \pm 0.14) \times 10^{-12}$ cm^3 molecule^{-1} s^{-1} (Debnath and Rajakumar, 2024), further validating the reliability

387 of the present computational protocol. To the best of our knowledge, no prior experimental or theoretical studies have reported

388 rate constants for the reactions of CH$_2$OO with pentanal or hexanal. Our calculations indicate that the rate constant for CH$_2$OO

389 + C$_4$H$_9$CHO is comparable to that for CH$_3$CHO, whereas the rate constant for CH$_2$OO + C$_5$H$_{11}$CHO is approximately twice as

390 large, yet remains within the same order of magnitude (Table 5). These results demonstrate that increasing alkyl chain length

391 exerts only a minor influence on the reaction kinetics of CH$_2$OO with aldehydes, revealing a weak and nonmonotonic size

392 dependence across the C$_1$–C$_5$ series. This behavior is fully consistent with the computed activation enthalpies (See Figure 1)

393 and establishes a transferable structure–reactivity relationship for CH$_2$OO reactions with larger aldehydes. Overall, aside from

394 formaldehyde, the rate constants for CH$_2$OO reactions with alkyl-substituted aldehydes vary only modestly, underscoring the

395 limited role of substituent size in governing CH$_2$OO reactivity.

396 ***The reaction of CH$_2$OO + RCHO (R=CH$_2$F/CHF$_2$/CHF$_3$).*** A striking fluorination-induced reactivity enhancement

397 emerges upon substitution of hydrogen atoms on the methyl group. Introduction of fluorine leads to a pronounced increase in

398 the rate constants for CH$_2$OO + CH$_3$CHO reactions, revealing an unexpected structure–reactivity trend. At 298 K, the rate

399 constant for reaction R7 is 1.31×10^{-11} cm^3 molecule^{-1} s^{-1} (Table 5), which is about 6 times larger than that of R2 and about 5

400 times larger than the corresponding OH + CH$_2$FCHO reaction (Lily et al., 2021).

401 Even more dramatic behavior is observed for reactions R8 and R9. For R8, the calculated rate constants approach the

402 collision limit, decreasing slightly from 4.51×10^{-10} cm^3 molecule^{-1} s^{-1} at 200 K to 6.75×10^{-11} cm^3 molecule^{-1} s^{-1} at 340 K

403 in Table 5, indicating of a weak negative temperature dependence characteristic of barrierless barrier processes. Notably, at

404 298 K the reaction of CHF$_2$CHO with CH$_2$OO is more than two orders of magnitude faster than its reactions with OH [$(1.8 \pm$

405 $0.4) \times 10^{-12}$ cm^3 molecule^{-1} s^{-1}] (Sellevåg et al., 2005), underscoring the unusually high reactivity of CH$_2$OO toward fluorinated

406 aldehydes.

407 The most pronounced effect is found for R9, for which the rate constant ranges from 7.40×10^{-10} cm^3 molecule^{-1} s^{-1} at

408 200 K to 5.76×10^{-10} cm^3 molecule^{-1} s^{-1} at 340 K in Table 5, fully approaching the collision limit and exceeding the

409 corresponding OH-initiated reaction rates by orders of magnitude. These results demonstrate that fluorination fundamentally

410 alters the reaction landscape of CH$_2$OO with aldehydes, transforming otherwise moderately fast bimolecular reactions into

411   near-collision-controlled processes.

3.6. Atmospheric Implications

413   The reaction of aldehydes with OH have been investigated extensively experimentally and theoretically. Here, we

414   considered the competition for aldehydes relative to CH_2OO and OH. the ratio of reaction rate was calculated by eqn (9):

$$v_i = \frac{k_i[CH_2OO]}{k_{OH,i}[OH]} \tag{9}$$

416   where the k_i is the rate constants for the reaction R2-R9, $k_{OH,i}$ is the rate constant of OH + RCHO (R = CH_3, C_2H_5, C_3H_7, C_4H_9,

417   C_5H_{11}, CH_2F, CHF_2, CF_3), and i is referred to is equal to 2-9. The concentrations of CH_2OO and OH exhibit pronounced

418   geographical and spatial distributions. The concentration of OH is varied from 10^4-10^6 molecules cm^{-3} (Khan et al., 2018; Ren

419   et al., 2003; Stone et al., 2012), and the estimated concentration for CH_2OO is range from 10^4 to 10^5 molecules cm^{-3} (peaking

420   at 6×10^5 molecules cm^{-3}) (Lelieveld et al., 2016; Novelli et al., 2017) In contrast, the base-version model simulations yield

421   CH_2OO concentrations approximately one order of magnitude lower than the estimated value. This discrepancy likely

422   originates from (i) the adoption of relatively fast rate constants for CH_2OO loss via reactions with H_2O and $(H_2O)_2$, and (ii) an

423   incomplete representation of CH_2OO sources in the model framework. Consequently, the use of model-derived concentrations

424   probably leads to an underestimation of the contribution of CH2OO to aldehyde removal.

425   Our results demonstrate that for aliphatic aldehydes, reactions with CH_2OO constitute a negligible sink compared with OH

426   oxidation, owing to both modest rate constants and low ambient CH_2OO concentration (See Tables S25–S27). Although

427   fluorine substitution generally enhances reactivity, the increase in the rate constant for CH_2FCHO remains insufficient to

428   meaningfully compete with the OH pathway. Effective competition is predicted only under highly specific conditions—namely,

429   nighttime at ~10 km altitude over the Malaysian region (Table 6). In stark contrast, the reactions of highly fluorinated aldehydes

430   with CH_2OO proceed at near-collision-limit rates. As a result, CH_2OO constitutes a major atmospheric sink for CHF_2CHO and

431   CF_3CHO. As summarized in Table 6, CH_2OO competes effectively with OH for CHF_2CHO at night near the surface over

432   Russia and the Arctic, influences its removal at 5 km over Russia and Indonesia, and contributes significantly at 10 km over

433   Indonesia. Notably, because the reaction of CF_3CHO with OH is intrinsically slow, CH_2OO dominates its atmospheric removal

434   over Indonesia at all altitudes considered, while in the Russian region its influence is confined to 0 and 5 km.

435   **Table 6.** rate concentration ratios CH$_2$OO to OH and the rate ratio at different heights from different region

Height	T/K	P/mBar	[CH$_2$OO]/[OH][a]	v_8[b]	v_9[c]
Gansu, China					
1	290.2	1013	2.48×10^{-4}	2.89×10^{-2}	2.29×10^{-1}
5	250.5	495.9	3.09×10^{-4}	6.25×10^{-2}	3.03×10^{-1}
10	215.6	242.8	3.51×10^{-5}	8.14×10^{-3}	3.77×10^{-2}
Russia					
1	290.2	1013	1.52×10^{-2}	1.77	14
5	250.5	495.9	6.39×10^{-3}	1.29	6.26
10	215.6	242.8	3.23×10^{-5}	7.48×10^{-3}	3.47×10^{-2}
Arctic					
1	290.2	1013	1.15×10^{-2}	1.33	10.6
5	250.5	495.9	5.16×10^{-4}	1.04×10^{-1}	5.05×10^{-1}
10	215.6	242.8	1.91×10^{-6}	4.43×10^{-4}	2.05×10^{-3}
Indonesia					
1	290.2	1013	3.16×10^{-3}	3.67×10^{-1}	2.91
5	250.5	495.9	5.85×10^{-3}	1.18	5.74
10	215.6	242.8	2.53×10^{-2}	5.87	27.2

436   [a]The concentration ratio between CH$_2$OO and OH from GEOS-Chem.

437   [b]The rate ratio between CH$_2$OO + CHF$_2$CHO and CHF$_2$CHO + OH.

438   [c]The rate ration between CH$_2$OO + CF$_3$CHO and CF$_3$CHO + OH.

439   Overall, these findings reveal a qualitative shift in aldehyde oxidation pathways upon heavy fluorination, identifying

440   CH$_2$OO as a previously underappreciated but potentially dominant oxidant for highly fluorinated aldehydes under specific

441   atmospheric regimes—an effect with important implications for the atmospheric lifetimes of emerging fluorinated oxygenated

442   VOCs.

443   **3.7. Atmospheric modelling**

444   Model simulations were further performed to assess the atmospheric significance of nighttime reactions between CH$_2$OO

445   and aldehydes. The Criegee intermediate (CI) chemistry implemented in the base model has been described in our previous

446   work (Long et al., 2024). In this study, two targeted updates were introduced to isolate and quantify the impacts of newly

447   identified CI–aldehyde reaction pathways. The first update incorporates the CH$_2$OO + HCHO reaction into the base mechanism,

448   reflecting an improved understanding of CI removal under aldehyde-rich nighttime conditions. The second update further

449   expands the CI sink by including the reaction between CH_2OO and CH_3CHO, thereby providing a more comprehensive

450   representation of acetaldehyde-driven CI loss. The aldehyde chemistry employed in the model is summarized in Table S28.

451   We do not consider the impact of CH_2OO on fluorinated aldehyde sinks by using GEOS-Chem, as fluorinated aldehydes are

452   not involved in the current default GEOS-Chem version.

453   The simulated aldehyde concentrations exhibit pronounced spatial and vertical heterogeneity. Surface-level HCHO

454   concentrations reach up to 1.46×10^{11} molecules cm^{-3}, while CH_3CHO attains maxima of 8.06×10^{10} molecules cm^{-3}, with

455   the highest abundances over Malaysia and Indonesia. These values are consistent with field observations, which report peak

456   HCHO concentrations of up to 3.63×10^{11} molecules cm^{-3} (Hu et al., 2025), lending confidence to the model performance.

457   The simulated global mean surface concentration of CH_3CHO (5.89×10^9 molecules cm^{-3}, corresponding to ~200 ppt) is in

458   reasonable agreement with observational constraints and remains lower than values reported by Komazaki et al (Komazaki et

459   al., 1999; Tereszchuk and Bernath, 2011).

460   The contribution of HCHO to the reduction of CH_2OO has been assessed in our prior work and is once again validated

461   by model simulations (Long et al., 2021). Figure 5 shows the relative changes in annual mean surface-layer CH_2OO

462   concentrations resulting from the inclusion of the CH_2OO + HCHO (R1) and CH_2OO + CH_3CHO (R2) reactions. Incorporation

463   of the updated rate constant for R1 leads to a pronounced reduction in CH_2OO, with a maximum decrease of 25.3% over the

464   Antarctic region (Figure 5), highlighting the previously unrecognized importance of HCHO as a nighttime CI sink. In contrast,

465   R2 produces a more modest effect, with a maximum CH_2OO reduction of 3.39% over Russia in Figure 5.

466
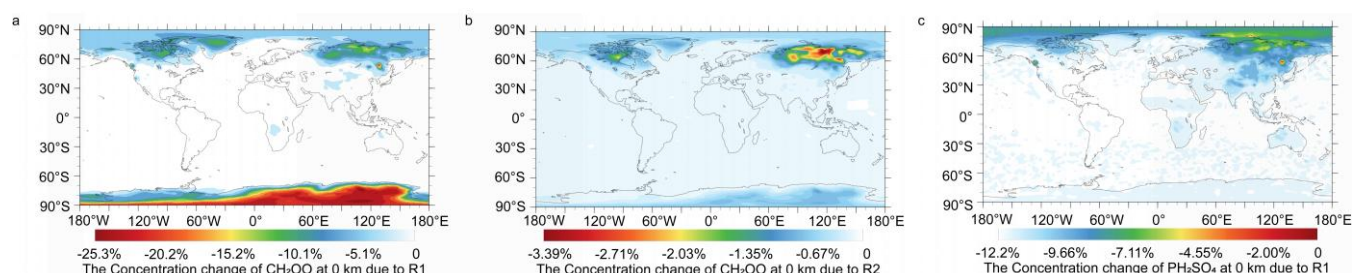
467   **Figure 5.** Changes in global CH_2OO concentrations due to reaction R1 and R2 (a) reaction R1, (b) reaction R2, and (c) changes

468   in global sulfate concentrations due to reaction R1.

469   Despite the substantial impact on CI abundances, the direct effects on aldehyde concentrations remain small. As shown in

470   Figure S8, surface acetaldehyde decreases by only 0.12% in the Arctic. However, the influence on secondary oxygenated

471   products is more pronounced. As illustrated in Figure S9, inclusion of R1 enhances formic acid concentrations by up to 5.44%

472   over Canada and Russia, while acetic acid increases by as much as 0.69% in the Arctic. These results demonstrate that CI–

473   aldehyde reactions, while exerting limited feedback on aldehydes themselves, can make significant contribution to the sinks

474   of CH_2OO and the formation of atmospheric acids.

475   The potential implications of reaction R1 for regional air quality were also assessed, particularly regarding the mitigation

476   of gas-phase sulfate formation. The inclusion of this reaction pathway effectively lowers the concentration of CH_2OO, thereby

477   diminishing its capacity to oxidize SO_2 into sulfuric acid precursors. This depletion of oxidative capacity leads to a marked

478   decrease in gas-phase sulfate concentration. The effect is geographical, with the reduction in gas-phase sulfate concentrations

479   estimated to be 12.2% in Canada and 6.01% in Russia during the nighttime. This indicates that the reaction plays a significant

480   role in the reduction of atmospheric sulfate aerosols.

481   **4. CONCLUSIONS**

482   The present work establishes a transferable and systematically improvable theoretical framework for predicting quantitative

483   atmospheric reaction kinetics across molecular complexity, using the reactions of CH_2OO with a series of aldehydes as a

484   definitive test case. By explicitly approaching the full configuration interaction (CI) limit for the benchmark CH_2OO + HCHO

485   system, we delineate the accuracy requirements necessary for reliable kinetic predictions and provide a rigorous reference

486   against which lower-cost methods can be assessed. Energetic and kinetic analyses validate a simplified reaction mechanism,

487   attributed to the facile interconversion between complexes and the energetic preference for rotational transition states over

488   addition pathways.

489   Guided by the detailed electronic-structure insights obtained for CH_2OO + HCHO, we develop a computational protocol

490   that integrates optimized geometries, vibrational frequencies, and high-level single-point energies, enabling accurate kinetics

491   for larger systems at feasible computational cost. We find that DF-CCSD(T)-F12b/VDZ(d) and DF-CCSD(T)-F12b/jun-cc-

492   pVDZ can be used to reliably describe the optimized geometries and calculated frequencies. two generalizable strategies (BE1

493 and BE2) have been used to recover the CCSDTQ/CBS level single point energies, which provide new insight into how to

494 obtain the quantitative enthalpy of activation.

495 In kinetics calculations, for reactions with appreciable barriers (R2–R6), this dual-level strategy yields robust rate

496 constants, whereas for reactions characterized by exceptionally low or submerged barriers (R1 and R7–R9), the explicit

497 application of VRC-VTST proves essential for capturing the correct dynamical behavior. This demonstrates a practical pathway

498 for extending benchmark-level kinetics from small to chemically diverse, larger molecules.

499 The resulting kinetic trends reveal that alkyl-chain elongation exerts only a minor influence on reactivity, whereas fluorine

500 substitution dramatically enhances reaction rates, driving the $CH_2OO + CHF_2CHO$ and $CH_2OO + CF_3CHO$ reactions toward

501 the collision limit. All reactions exhibit negligible pressure dependence, underscoring their relevance under atmospheric

502 conditions. These high-precision rate constants provide a mechanistically grounded explanation for the increasingly important

503 role of Criegee intermediates in the oxidation of fluorinated aldehydes. We find that fluorine substitution on aldehydes

504 dramatically enhances their reactivity toward CH_2OO; however, the post-CCSD(T) contributions remain almost equal across

505 the reaction series. This behavior indicates that fluorination-driven rate acceleration is governed primarily by lower-level

506 electronic effects rather than by higher-order electron correlation than CCSD(T). This observation also provides a fundamental

507 basis for the development of high-accuracy semiempirical correction schemes.

508 Beyond molecular-scale kinetics, global and regional modeling demonstrates that while reactions of CH_2OO with HCHO

509 and CH_3CHO contribute negligibly to aldehyde removal, HCHO constitutes a major global sink for Criegee intermediates,

510 accounting for a 25.3% reduction in the global CH_2OO burden during the night. In contrast, fluorination fundamentally alters

511 atmospheric fate: for CH_2FCHO, CH_2OO reactions become regionally significant (e.g., near 10 km altitude over Malaysia),

512 and for more heavily fluorinated aldehydes such as CHF_2CHO, CH_2OO overwhelmingly dominates over OH-initiated loss

513 pathways. The associated enhancement in acid formation, although modest, further highlights the chemical implications of

514 these processes. The inclusion of reaction R1 results in a reduction of gas-phase sulfate levels by 12.2% over Canada and 6.01%

515 over Russia. These present findings deliver a generalizable, benchmark-anchored strategy for quantitative kinetic prediction,

516 bridges electronic-structure theory with atmospheric modeling, and reveals how fluorination reshapes the atmospheric

517 relevance of Criegee intermediates—insights that are critical for atmospheric chemical mechanisms.

Supplement. The following information is provided in the Supplement: Details of reaction R9, enthalpies of binding and activation and barrier height; vibrational frequency scale factors; Lennard-Jone parameters; Rate constants and rate constant fits; Rate ratio; Absolute energies and the Cartesian coordinates and absolute energies; relative enthalpies for reaction of R3-R9; Enthalpy profile for the conversion of pre-reaction complex; Changes in global CH_3CHO, $HCOOH$, and CH_3COOH concentrations.

Data and code availability. Electronic structure calculations were performed using commercially available software (Gaussian 16, Revision A.03 and Molpro 2019). Access to the software is subject to licensing terms. The MRCC and MSTor codes can be accessed at https://www.mrcc.hu and https://comp.chem.umn.edu/mstor, respectively. Polyrate 2017-C and Gaussrate 2017-B are available at https://comp.chem.umn.edu/polyrate and https://comp.chem.umn.edu/gaussrate. KiSThlP 2021 is accessible at http://kisthelp.univ-reims.fr, and the TUMME program can be found at https://comp.chem.umn.edu/tumme. The GEOS-Chem 14.4.2 is available at http://www.geos-chem.org. Optimized geometries, and calculated energies are available in Supplement. Other data are available from the corresponding author upon reasonable request.

Author contributions. CX carried out the calculations, analysed and interpretation of data, and wrote the manuscript draft. BL designed the project, analysed and inerpretation of data, and reviewed and edited the manuscript.

Competing interests. The authors declare that they have no conflict of interest.

Reference

Adler, T. B., Knizia, G., and Werner, H.-J.: A simple and efficient CCSD(T)-F12 approximation, J. Chem. Phys., 127, 221106, https://doi.org/10.1063/1.2817618, 2007.

Atkinson, R. and Pitts, J. N., Jr.: Kinetics of the reactions of the OH radical with HCHO and CH_3CHO over the temperature range 299–426 K, J. Chem. Phys., 68, 3581-3584, https://doi.org/10.1063/1.436215, 1978.

Bao, J., Zhang, X., Wu, Z., Zhou, L., Qian, J., Tan, Q., Yang, F., Chen, J., Li, Y., Liu, H., Deng, L., and Li, H.: Atmospheric carbonyl compounds are crucial in regional ozone heavy pollution: insights from the Chengdu Plain Urban Agglomeration, China, Atmos. Chem. Phys., 25, 1899-1916, https://doi.org/10.5194/acp-25-1899-2025, 2025.

Bao, J. L., Zhang, X., and Truhlar, D. G.: Predicting pressure-dependent unimolecular rate constants using variational transition state theory with multidimensional tunneling combined with system-specific quantum RRK theory: a definitive test for fluoroform dissociation, Phys. Chem. Chem. Phys., 18, 16659-16670, https://doi.org/10.1039/C6CP02765B, 2016a.

Bao, J. L., Zhang, X., and Truhlar, D. G.: Barrierless association of CF_2 and dissociation of C_2F_4 by variational transition-state theory and system-specific quantum Rice–Ramsperger–Kassel theory, Proc. Natl. Acad. Sci., 113, 13606-13611, https://doi.org/10.1073/pnas.1616208113, 2016b.

Bari, M. A. and Kindzierski, W. B.: Ambient volatile organic compounds (VOCs) in Calgary, Alberta: Sources and screening health risk assessment, Sci. Total Environ., 631-632, 627-640, https://doi.org/10.1016/j.scitotenv.2018.03.023, 2018.

Berndt, T., Jokinen, T., Sipilä, M., Mauldin, R. L., Herrmann, H., Stratmann, F., Junninen, H., and Kulmala, M.: H_2SO_4 formation from the gas-phase reaction of stabilized Criegee Intermediates with SO_2: Influence of water vapour content and temperature, Atmos. Environ., 89, 603-612, https://doi.org/10.1016/j.atmosenv.2014.02.062, 2014.

Berndt, T., Kaethner, R., Voigtländer, J., Stratmann, F., Pfeifle, M., Reichle, P., Sipilä, M., Kulmala, M., and Olzmann, M.: Kinetics of the unimolecular reaction of CH_2OO and the bimolecular reactions with the water monomer, acetaldehyde and acetone under atmospheric conditions, Phys. Chem. Chem. Phys., 17, 19862-19873, https://doi.org/10.1039/C5CP02224J, 2015.

Bey, I., Jacob, D. J., Yantosca, R. M., Logan, J. A., Field, B. D., Fiore, A. M., Li, Q., Liu, H. Y., Mickley, L. J., and Schultz, M. G.: Global modeling of tropospheric chemistry with assimilated meteorology: Model description and evaluation, J. Geophys. Res.: Atmos., 106, 23073-23095, https://doi.org/10.1029/2001JD000807, 2001.

Bischoff, F. A., Wolfsegger, S., Tew, D. P., and Klopper, W.: Assessment of basis sets for F12 explicitly-correlated molecular electronic-structure methods, Mol. Phys., 107, 963-975, https://doi.org/10.1080/00268970802708942, 2009.

Bossmeyer, J., Brauers, T., Richter, C., Rohrer, F., Wegener, R., and Wahner, A.: Simulation chamber studies on the NO_3 chemistry of atmospheric aldehydes, Geophys. Res. Lett., 33, https://doi.org/10.1029/2006GL026778, 2006.

Boy, M., Mogensen, D., Smolander, S., Zhou, L., Nieminen, T., Paasonen, P., Plass-Dülmer, C., Sipilä, M., Petäjä, T., Mauldin, L., Berresheim, H., and Kulmala, M.: Oxidation of SO_2 by stabilized Criegee intermediate (sCI) radicals as a crucial source for atmospheric sulfuric acid concentrations, Atmos. Chem. Phys., 13, 3865-3879, https://doi.org/10.5194/acp-13-3865-2013, 2013.

580   Cabañas, B., Martín, P., Salgado, S., Ballesteros, B., and Martínez, E.: An Experimental Study on the Temperature Dependence

581   for the Gas-Phase Reactions of NO_3 Radical with a Series of Aliphatic Aldehydes, J. Atmos. Chem., 40, 23-39,

582   https://doi.org/10.1023/A:1010797424283, 2001.

583   Cabezas, C. and Endo, Y.: The Criegee intermediate-formic acid reaction explored by rotational spectroscopy, Phys. Chem.

584   Chem. Phys., 21, 18059-18064, https://doi.org/10.1039/C9CP03001H, 2019.

585   Canneaux, S., Bohr, F., and Henon, E.: KiSThelP: A program to predict thermodynamic properties and rate constants from

586   quantum chemistry results, J. Comput. Chem., 35, 82-93, https://doi.org/10.1002/jcc.23470, 2014.

587   Chan, B. and Radom, L.: W2X and W3X-L: Cost-Effective Approximations to W2 and W4 with kJ mol^{-1} Accuracy, J. Chem.

588   Theory Comput., 11, 2109-2119, https://doi.org/10.1021/acs.jctc.5b00135, 2015.

589   Chandra, A. K., Uchimaru, T., and Sugie, M.: Kinetics of hydrogen abstraction reactions of CF_3CHO, CF_2ClCHO, $CFCl_2CHO$

590   and CCl_3CHO with OH Radicals: An ab initio study, Phys. Chem. Chem. Phys., 3, 3961-3966,

591   https://doi.org/10.1039/B104904F, 2001.

592   Chen, W. T., Shao, M., Lu, S. H., Wang, M., Zeng, L. M., Yuan, B., and Liu, Y.: Understanding primary and secondary sources

593   of ambient carbonyl compounds in Beijing using the PMF model, Atmos. Chem. Phys., 14, 3047-3062,

594   https://doi.org/10.5194/acp-14-3047-2014, 2014.

595   Chhantyal-Pun, R., Khan, M. A. H., Zachhuber, N., Percival, C. J., Shallcross, D. E., and Orr-Ewing, A. J.: Impact of Criegee

596   Intermediate Reactions with Peroxy Radicals on Tropospheric Organic Aerosol, ACS Earth Space Chem., 4, 1743-1755,

597   https://doi.org/10.1021/acsearthspacechem.0c00147, 2020.

598   Chung, C.-A., Su, J. W., and Lee, Y.-P.: Detailed mechanism and kinetics of the reaction of Criegee intermediate CH_2OO with

599   HCOOH investigated via infrared identification of conformers of hydroperoxymethyl formate and formic acid anhydride, Phys.

600   Chem. Chem. Phys., 21, 21445-21455, https://doi.org/10.1039/C9CP04168K, 2019.

601   Cornwell, Z. A., Enders, J. J., Harrison, A. W., and Murray, C.: Temperature-dependent kinetics of the reactions of CH_2OO

602   with acetone, biacetyl, and acetylacetone, Int. J. Chem. Kinet., 55, 154-166, https://doi.org/10.1002/kin.21625, 2023.

603   Criegee, R.: Mechanism of Ozonolysis, Angew. Chem. Int. Ed., 14, 745-752, https://doi.org/10.1002/anie.197507451, 1975.

604   Criegee, R. and Wenner, G.: Die Ozonisierung des 9,10-Oktalins, Justus Liebigs Ann. Chem., 564, 9-15,

605   https://doi.org/10.1002/jlac.19495640103, 1949.

606   D'Anna, B., Andresen, Ø., Gefen, Z., and Nielsen, C. J.: Kinetic study of OH and NO_3 radical reactions with 14 aliphatic

607   aldehydes, Phys. Chem. Chem. Phys., 3, 3057-3063, https://doi.org/10.1039/B103623H, 2001.

608   Debnath, A. and Rajakumar, B.: Experimental and theoretical study of Criegee intermediate (CH_2OO) reactions with n-

609   butyraldehyde and isobutyraldehyde: kinetics, implications and atmospheric fate, Phys. Chem. Chem. Phys., 26, 6872-6884,

610   https://doi.org/10.1039/D3CP05482A, 2024.

611   Ding, D.-P. and Long, B.: Reaction between propionaldehyde and hydroxyperoxy radical in the atmosphere: A reaction route

612   for the sink of propionaldehyde and the formation of formic acid, Atmos. Environ., 284, 119202,

613   https://doi.org/10.1016/j.atmosenv.2022.119202, 2022.

614   Edwards, P. M., Brown, S. S., Roberts, J. M., Ahmadov, R., Banta, R. M., deGouw, J. A., Dubé, W. P., Field, R. A., Flynn, J.

615   H., Gilman, J. B., Graus, M., Helmig, D., Koss, A., Langford, A. O., Lefer, B. L., Lerner, B. M., Li, R., Li, S.-M., McKeen, S.

616   A., Murphy, S. M., Parrish, D. D., Senff, C. J., Soltis, J., Stutz, J., Sweeney, C., Thompson, C. R., Trainer, M. K., Tsai, C.,

617 Veres, P. R., Washenfelder, R. A., Warneke, C., Wild, R. J., Young, C. J., Yuan, B., and Zamora, R.: High winter ozone pollution
618 from carbonyl photolysis in an oil and gas basin, Nature, 514, 351-354, https://doi.org/10.1038/nature13767, 2014.

619 Elsamra, R. M. I., Jalan, A., Buras, Z. J., Middaugh, J. E., and Green, W. H.: Temperature- and Pressure-Dependent Kinetics
620 of CH_2OO + CH_3COCH_3 and CH_2OO + CH_3CHO: Direct Measurements and Theoretical Analysis, Int. J. Chem. Kinet., 48,
621 474-488, https://doi.org/10.1002/kin.21007, 2016.

622 Enders, J. J., Cornwell, Z. A., Harrison, A. W., and Murray, C.: Temperature-Dependent Kinetics of the Reactions of the Criegee
623 Intermediate CH_2OO with Aliphatic Aldehydes, J. Phys. Chem. A, 128, 7879-7888, https://doi.org/10.1021/acs.jpca.4c04990,
624 2024.

625 Fernández-Ramos, A., Miller, J. A., Klippenstein, S. J., and Truhlar, D. G.: Modeling the Kinetics of Bimolecular Reactions,
626 Chem. Rev., 106, 4518-4584, https://doi.org/10.1021/cr050205w, 2006.

627 Foreman, E. S., Kapnas, K. M., and Murray, C.: Reactions between Criegee Intermediates and the Inorganic Acids HCl and
628 HNO3:   Kinetics   and   Atmospheric   Implications,   Angew.   Chem.   Int.   Ed.,   55,   10419-10422,
629 https://doi.org/10.1002/anie.201604662, 2016.

630 Frisch, M. J., Trucks, G. W., Schlegel, H. B., Scuseria, G. E., Robb, M. A., Cheeseman, J. R., Scalmani, G., Barone, V.,
631 Mennucci, B., Petersson, G. A., Nakatsuji, H., Caricato, M., Li, X., Hratchian, H. P., Izmaylov, A. F., Bloino, J., Zheng, G.,
632 Sonnenberg, J. L., Hada, M., Ehara, M., Toyota, K., Fukuda, ., Hasegawa, J., Ishida, M., Nakajima, T., Honda, Y., Kitao, O.,
633 Nakai, H., Vreven, T., Montgomery, J. A., Peralta, J. E., Ogliaro, F., Bearpark, M., Heyd, J. J., Brothers, E., Kudin, K. N.,
634 Staroverov, V. N., Kobayashi, R., Normand, J., Raghavachari, K., Rendell, A., Burant, J. C., Iyengar, S. S., Tomasi, J., Cossi,
635 M., Rega, N., Millam, J. M., Klene, M., Knox, J. E., Cross, J. B., Bakken, V., Adamo, C., Jaramillo, J., Gomperts, R., Stratmann,
636 R. E., Yazyev, O., Austin, A. J., Cammi, R., Pomelli, C., Ochterski, J. W., Martin, R. L., Morokuma, K., Zakrzewski, V. G.,
637 Voth, G. A., Salvador, P., Dannenberg, J. J., Dapprich, S., Daniels, A. D., Farkas, O., Foresman, J. B., Ortiz, J. V., Cioslowski,
638 J., and Fox, D. J.: Gaussian 16, Revision A.03, Gaussian Inc, Wallingford CT, https://gaussian.com/gaussian16/ (last access:
639 20 November 2023), 2016.

640 Gao, Q., Shen, C., Zhang, H., Long, B., and Truhlar, D. G.: Quantitative kinetics reveal that reactions of HO_2 are a significant
641 sink for aldehydes in the atmosphere and may initiate the formation of highly oxygenated molecules via autoxidation, Phys.
642 Chem. Chem. Phys., 26, 16160-16174, https://doi.org/10.1039/D4CP00693C, 2024.

643 Garrett, B. C. and Truhlar, D. G.: Canonical unified statistical model. Classical mechanical theory and applications to collinear
644 reactions, J. Chem. Phys., 76, 1853-1858, https://doi.org/10.1063/1.443157, 1982.

645 Gelaro, R., McCarty, W., Suárez, M. J., Todling, R., Molod, A., Takacs, L., Randles, C. A., Darmenov, A., Bosilovich, M. G.,
646 Reichle, R., Wargan, K., Coy, L., Cullather, R., Draper, C., Akella, S., Buchard, V., Conaty, A., da Silva, A. M., Gu, W., Kim,
647 G.-K., Koster, R., Lucchesi, R., Merkova, D., Nielsen, J. E., Partyka, G., Pawson, S., Putman, W., Rienecker, M., Schubert, S.
648 D., Sienkiewicz, M., and Zhao, B.: The Modern-Era Retrospective Analysis for Research and Applications, Version 2
649 (MERRA-2), J. Clim., 30, 5419-5454, https://doi.org/10.1175/JCLI-D-16-0758.1, 2017.

650 Georgievskii, Y. and Klippenstein, S. J.: Variable reaction coordinate transition state theory: Analytic results and application
651 to the C_2H_3+H→C_2H_4 reaction, J. Chem. Phys., 118, 5442-5455, https://doi.org/10.1063/1.1539035, 2003.

652 Georgievskii, Y., Miller, J. A., Burke, M. P., and Klippenstein, S. J.: Reformulation and Solution of the Master Equation for
653 Multiple-Well Chemical Reactions, J. Phys. Chem. A, 117, 12146-12154, https://doi.org/10.1021/jp4060704, 2013.

654   Grosjean, D., Swanson, R. D., and Ellis, C.: Carbonyls in Los Angeles air: Contribution of direct emissions and photochemistry,
655   Sci. Total Environ., 29, 65-85, https://doi.org/10.1016/0048-9697(83)90034-7, 1983.

656   Guenther, A. B., Jiang, X., Heald, C. L., Sakulyanontvittaya, T., Duhl, T., Emmons, L. K., and Wang, X.: The Model of
657   Emissions of Gases and Aerosols from Nature version 2.1 (MEGAN2.1): an extended and updated framework for modeling
658   biogenic emissions, Geosci. Model Dev., 5, 1471-1492, https://doi.org/10.5194/gmd-5-1471-2012, 2012.

659   Győrffy, W. and Werner, H.-J.: Analytical energy gradients for explicitly correlated wave functions. II. Explicitly correlated
660   coupled cluster singles and doubles with perturbative triples corrections: CCSD(T)-F12, J. Chem. Phys., 148, 114104,
661   https://doi.org/10.1063/1.5020436, 2018.

662   Hoesly, R. M., Smith, S. J., Feng, L., Klimont, Z., Janssens-Maenhout, G., Pitkanen, T., Seibert, J. J., Vu, L., Andres, R. J.,
663   Bolt, R. M., Bond, T. C., Dawidowski, L., Kholod, N., Kurokawa, J. I., Li, M., Liu, L., Lu, Z., Moura, M. C. P., O'Rourke, P.
664   R., and Zhang, Q.: Historical (1750–2014) anthropogenic emissions of reactive gases and aerosols from the Community
665   Emissions Data System (CEDS), Geosci. Model Dev., 11, 369-408, https://doi.org/10.5194/gmd-11-369-2018, 2018.

666   Hu, R., Zhang, G., Cai, H., Guo, J., Lu, K., Li, X., Lou, S., Tan, Z., Hu, C., Xie, P., and Liu, W.: Accurate elucidation of
667   oxidation under heavy ozone pollution: a full suite of radical measurements in the chemically complex atmosphere, Atmos.
668   Chem. Phys., 25, 3011-3028, https://doi.org/10.5194/acp-25-3011-2025, 2025.

669   Jalan, A., Allen, J. W., and Green, W. H.: Chemically activated formation of organic acids in reactions of the Criegee
670   intermediate with aldehydes and ketones, Phys. Chem. Chem. Phys., 15, 16841-16852, https://doi.org/10.1039/C3CP52598H,
671   2013.

672   Jenkin, M. E., Valorso, R., Aumont, B., Rickard, A. R., and Wallington, T. J.: Estimation of rate coefficients and branching
673   ratios for gas-phase reactions of OH with aromatic organic compounds for use in automated mechanism construction, Atmos.
674   Chem. Phys., 18, 9329-9349, https://doi.org/10.5194/acp-18-9329-2018, 2018.

675   Jiang, H., Liu, Y., Xiao, C., Yang, X., and Dong, W.: Reaction Kinetics of CH_2OO and syn-CH_3CHOO Criegee Intermediates
676   with Acetaldehyde, J. Phys. Chem. A, 128, 4956-4965, https://doi.org/10.1021/acs.jpca.4c01374, 2024.

677   Jiménez, E., Lanza, B., Martínez, E., and Albaladejo, J.: Daytime tropospheric loss of hexanal and trans-2-hexenal: OH kinetics
678   and UV photolysis, Atmos. Chem. Phys., 7, 1565-1574, https://doi.org/10.5194/acp-7-1565-2007, 2007.

679   Kaipara, R. and Rajakumar, B.: Temperature-Dependent Kinetics of the Reaction of a Criegee Intermediate with
680   Propionaldehyde: A Computational Investigation, J. Phys. Chem. A, 122, 8433-8445, https://doi.org/10.1021/acs.jpca.8b06603,
681   2018.

682   Kállay, M., Nagy, P. R., Mester, D., Rolik, Z., Samu, G., Csontos, J., Csóka, J., Szabó, P. B., Gyevi-Nagy, L., Hégely, B.,
683   Ladjánszki, I., Szegedy, L., Ladóczki, B., Petrov, K., Farkas, M., Mezei, P. D., and Ganyecz, Á.: The MRCC program system:
684   Accurate quantum chemistry from water to proteins, J. Chem. Phys., 152, 074107, https://doi.org/10.1063/1.5142048, 2020.

685   Kenneth A. Holbrook, M. J. P., Struan H. Robertson Unimolecular Reactions, 2nd ed., John Wiley & Sons: Chichester, pp,
686   177− 214, 1996.

687   Khan, M. A. H., Percival, C. J., Caravan, R. L., Taatjes, C. A., and Shallcross, D. E.: Criegee intermediates and their impacts
688   on the troposphere, Environ. Sci. Processes Impacts, 20, 437-453, https://doi.org/10.1039/C7EM00585G, 2018.

689   Klippenstein, S. J.: RRKM theory and its implementation, in: Comprehensive Chemical Kinetics, Elsevier, pp, 55-103, 2003.

690   Knizia, G., Adler, T. B., and Werner, H.-J.: Simplified CCSD(T)-F12 methods: Theory and benchmarks, J. Chem. Phys., 130,

691   054104, 10.1063/1.3054300, 2009.

692   Knote, C., Hodzic, A., Jimenez, J. L., Volkamer, R., Orlando, J. J., Baidar, S., Brioude, J., Fast, J., Gentner, D. R., Goldstein,

693   A. H., Hayes, P. L., Knighton, W. B., Oetjen, H., Setyan, A., Stark, H., Thalman, R., Tyndall, G., Washenfelder, R., Waxman,

694   E., and Zhang, Q.: Simulation of semi-explicit mechanisms of SOA formation from glyoxal in aerosol in a 3-D model, Atmos.

695   Chem. Phys., 14, 6213-6239, https://doi.org/10.5194/acp-14-6213-2014, 2014.

696   Komazaki, Y., Hiratsuka, M., Narita, Y., Tanaka, S., and Fujita, T.: The development of an automated continuous measurement

697   system for the monitoring of HCHO and CH_3CHO in the atmosphere by using an annular diffusion scrubber coupled to HPLC,

698   Fresenius' J. Anal. Chem., 363, 686-695, https://doi.org/10.1007/s002160051272, 1999.

699   Kukui, A., Chartier, M., Wang, J., Chen, H., Dusanter, S., Sauvage, S., Michoud, V., Locoge, N., Gros, V., Bourrianne, T.,

700   Sellegri, K., and Pichon, J. M.: Role of Criegee intermediates in the formation of sulfuric acid at a Mediterranean (Cape Corsica)

701   site under influence of biogenic emissions, Atmos. Chem. Phys., 21, 13333-13351, https://doi.org/10.5194/acp-21-13333-2021,

702   2021.

703   Lary, D. J. and Shallcross, D. E.: Central role of carbonyl compounds in atmospheric chemistry, J. Geophys. Res.: Atmos., 105,

704   19771-19778, https://doi.org/10.1029/1999JD901184, 2000.

705   Lelieveld, J., Gromov, S., Pozzer, A., and Taraborrelli, D.: Global tropospheric hydroxyl distribution, budget and reactivity,

706   Atmos. Chem. Phys., 16, 12477-12493, https://doi.org/10.5194/acp-16-12477-2016, 2016.

707   Li, F., Tang, S., Lv, J., Yu, S., Sun, X., Cao, D., Wang, Y., and Jiang, G.: Critical contribution of chemically diverse carbonyl

708   molecules to the oxidative potential of atmospheric aerosols, Atmos. Chem. Phys., 24, 8397-8411, https://doi.org/10.5194/acp-

709   24-8397-2024, 2024.

710   Lily, M., Hynniewta, S., Muthiah, B., Wang, W., Chandra, A. K., and Liu, F.: Quantum chemical insights into the atmospheric

711   reactions of CH2FCH2OH with OH radical, fate of $CH_2FC \cdot HOH$ radical and ozone formation potential, Atmos. Environ., 249,

712   118247, https://doi.org/10.1016/j.atmosenv.2021.118247, 2021.

713   Lin, H., Jacob, D. J., Lundgren, E. W., Sulprizio, M. P., Keller, C. A., Fritz, T. M., Eastham, S. D., Emmons, L. K., Campbell,

714   P. C., Baker, B., Saylor, R. D., and Montuoro, R.: Harmonized Emissions Component (HEMCO) 3.0 as a versatile emissions

715   component for atmospheric models: application in the GEOS-Chem, NASA GEOS, WRF-GC, CESM2, NOAA GEFS-Aerosol,

716   and NOAA UFS models, Geosci. Model Dev., 14, 5487-5506, https://doi.org/10.5194/gmd-14-5487-2021, 2021.

717   Liu, Q., Gao, Y., Huang, W., Ling, Z., Wang, Z., and Wang, X.: Carbonyl compounds in the atmosphere: A review of abundance,

718   source   and   their   contributions   to O_3 and   SOA   formation,   Atmos.   Res.,   274,   106184,

719   https://doi.org/10.1016/j.atmosres.2022.106184, 2022.

720   Liu, S., Chen, Y., Jiang, H., Shi, J., Ding, H., Yang, X., and Dong, W.: Reaction between Criegee Intermediate CH_2OO and

721   Isobutyraldehyde: Kinetics   and   Atmospheric   Implications,   ChemistrySelect,   8,   e202303129,

722   https://doi.org/10.1002/slct.202303129, 2023.

723   Liu, Y., Zhou, X., Chen, Y., Chen, M., Xiao, C., Dong, W., and Yang, X.: Temperature- and pressure-dependent rate coefficient

724   measurement   for   the   reaction   of   CH2OO   with CH_3CH_2CHO,   Phys.   Chem.   Chem.   Phys.,   22,   25869-25875,

725   https://doi.org/10.1039/D0CP04316H, 2020.

726   Long, B., Bao, J. L., and Truhlar, D. G.: Atmospheric Chemistry of Criegee Intermediates: Unimolecular Reactions and

727   Reactions with Water, J. Am. Chem. Soc., 138, 14409-14422, https://doi.org/10.1021/jacs.6b08655, 2016.

728 Long, B., Bao, J. L., and Truhlar, D. G.: Kinetics of the Strongly Correlated $CH_3O + O_2$ Reaction: The Importance of Quadruple
729 Excitations in Atmospheric and Combustion Chemistry, J. Am. Chem. Soc., 141, 611-617,
730 https://doi.org/10.1021/jacs.8b11766, 2019.

731 Long, B., Xia, Y., and Truhlar, D. G.: Quantitative Kinetics of HO_2 Reactions with Aldehydes in the Atmosphere: High-Order
732 Dynamic Correlation, Anharmonicity, and Falloff Effects Are All Important, J. Am. Chem. Soc., 144, 19910-19920,
733 https://doi.org/10.1021/jacs.2c07994, 2022.

734 Long, B., Xie, C., and Truhlar, D. G.: Criegee Intermediates Compete Well with OH as a Cleaning Agent for Atmospheric
735 Amides, J. Am. Chem. Soc., 147, 22237-22244, https://doi.org/10.1021/jacs.5c07439, 2025.

736 Long, B., Xia, Y., Zhang, Y.-Q., and Truhlar, D. G.: Kinetics of Sulfur Trioxide Reaction with Water Vapor to Form
737 Atmospheric Sulfuric Acid, J. Am. Chem. Soc., 145, 19866-19876, https://doi.org/10.1021/jacs.3c06032, 2023.

738 Long, B., Zhang, Y.-Q., Xie, C.-L., Tan, X.-F., and Truhlar, D. G.: Reaction of Carbonyl Oxide with Hydroperoxymethyl
739 Thioformate: Quantitative Kinetics and Atmospheric Implications, Research, 7, 0525, https://doi.org/10.34133/research.0525,
740 2024.

741 Long, B., Wang, Y., Xia, Y., He, X., Bao, J. L., and Truhlar, D. G.: Atmospheric Kinetics: Bimolecular Reactions of Carbonyl
742 Oxide by a Triple-Level Strategy, J. Am. Chem. Soc., 143, 8402-8413, https://doi.org/10.1021/jacs.1c02029, 2021.

743 Luecken, D. J., Hutzell, W. T., Strum, M. L., and Pouliot, G. A.: Regional sources of atmospheric formaldehyde and
744 acetaldehyde, and implications for atmospheric modeling, Atmos. Environ., 47, 477-490,
745 https://doi.org/10.1016/j.atmosenv.2011.10.005, 2012.

746 Luo, P.-L., Chen, I. Y., Khan, M. A. H., and Shallcross, D. E.: Direct gas-phase formation of formic acid through reaction of
747 Criegee intermediates with formaldehyde, Commun. Chem., 6, 130, https://doi.org/10.1038/s42004-023-00933-2, 2023.

748 Lynch, B. J., Zhao, Y., and Truhlar, D. G.: Effectiveness of Diffuse Basis Functions for Calculating Relative Energies by
749 Density Functional Theory, J. Phys. Chem. A, 107, 1384-1388, https://doi.org/10.1021/jp021590l, 2003.

750 Manonmani, G., Sandhiya, L., and Senthilkumar, K.: Reaction of Criegee Intermediates with SO2—A Possible Route for
751 Sulfurous Acid Formation in the Atmosphere, ACS Earth Space Chem., 7, 1890-1904,
752 https://doi.org/10.1021/acsearthspacechem.3c00058, 2023.

753 Mellouki, A., Wallington, T. J., and Chen, J.: Atmospheric Chemistry of Oxygenated Volatile Organic Compounds: Impacts on
754 Air Quality and Climate, Chem. Rev., 115, 3984-4014, https://doi.org/10.1021/cr500549n, 2015.

755 Novelli, A., Vereecken, L., Lelieveld, J., and Harder, H.: Direct observation of OH formation from stabilised Criegee
756 intermediates, Phys. Chem. Chem. Phys., 16, 19941-19951, https://doi.org/10.1039/C4CP02719A, 2014.

757 Novelli, A., Hens, K., Tatum Ernest, C., Martinez, M., Nölscher, A. C., Sinha, V., Paasonen, P., Petäjä, T., Sipilä, M., Elste, T.,
758 Plass-Dülmer, C., Phillips, G. J., Kubistin, D., Williams, J., Vereecken, L., Lelieveld, J., and Harder, H.: Estimating the
759 atmospheric concentration of Criegee intermediates and their possible interference in a FAGE-LIF instrument, Atmos. Chem.
760 Phys., 17, 7807-7826, https://doi.org/10.5194/acp-17-7807-2017, 2017.

761 Papagni, C., Arey, J., and Atkinson, R.: Rate constants for the gas-phase reactions of a series of C3-C6 aldehydes with OH and
762 NO_3 radicals, Int. J. Chem. Kinet., 32, 79-84, https://doi.org/10.1002/(SICI)1097-4601(2000)32:2<79::AID-KIN2>3.0.CO;2-
763 A, 2000.

764 Parker, T. M., Burns, L. A., Parrish, R. M., Ryno, A. G., and Sherrill, C. D.: Levels of symmetry adapted perturbation theory

765 (SAPT). I. Efficiency and performance for interaction energies, J. Chem. Phys., 140, 094106,
766 https://doi.org/10.1063/1.4867135, 2014.

767 Parrish, D. D., Ryerson, T. B., Mellqvist, J., Johansson, J., Fried, A., Richter, D., Walega, J. G., Washenfelder, R. A., de Gouw,
768 J. A., Peischl, J., Aikin, K. C., McKeen, S. A., Frost, G. J., Fehsenfeld, F. C., and Herndon, S. C.: Primary and secondary
769 sources of formaldehyde in urban atmospheres: Houston Texas region, Atmos. Chem. Phys., 12, 3273-3288,
770 https://doi.org/10.5194/acp-12-3273-2012, 2012.

771 Peltola, J., Seal, P., Inkilä, A., and Eskola, A.: Time-resolved, broadband UV-absorption spectrometry measurements of Criegee
772 intermediate kinetics using a new photolytic precursor: unimolecular decomposition of CH_2OO and its reaction with formic
773 acid, Phys. Chem. Chem. Phys., 22, 11797-11808, https://doi.org/10.1039/D0CP00302F, 2020.

774 Percival, C. J., Welz, O., Eskola, A. J., Savee, J. D., Osborn, D. L., Topping, D. O., Lowe, D., Utembe, S. R., Bacak, A., M c
775 Figgans, G., Cooke, M. C., Xiao, P., Archibald, A. T., Jenkin, M. E., Derwent, R. G., Riipinen, I., Mok, D. W. K., Lee, E. P. F.,
776 Dyke, J. M., Taatjes, C. A., and Shallcross, D. E.: Regional and global impacts of Criegee intermediates on atmospheric
777 sulphuric acid concentrations and first steps of aerosol formation, Faraday Discuss., 165, 45-73,
778 https://doi.org/10.1039/C3FD00048F, 2013.

779 Peverati, R. and Truhlar, D. G.: M11-L: A Local Density Functional That Provides Improved Accuracy for Electronic Structure
780 Calculations in Chemistry and Physics, J. Phys. Chem. Lett., 3, 117-124, https://doi.org/10.1021/jz201525m, 2012.

781 Raghunath, P., Lee, Y.-P., and Lin, M. C.: Computational Chemical Kinetics for the Reaction of Criegee Intermediate CH_2OO
782 with HNO_3 and Its Catalytic Conversion to OH and HCO, J. Phys. Chem. A, 121, 3871-3878,
783 https://doi.org/10.1021/acs.jpca.7b02196, 2017.

784 Ren, X., Harder, H., Martinez, M., Lesher, R. L., Oliger, A., Shirley, T., Adams, J., Simpas, J. B., and Brune, W. H.: HOx
785 concentrations and OH reactivity observations in New York City during PMTACS-NY2001, Atmos. Environ., 37, 3627-3637,
786 https://doi.org/10.1016/S1352-2310(03)00460-6, 2003.

787 Scollard, D. J., Treacy, J. J., Sidebottom, H. W., Balestra-Garcia, C., Laverdet, G., LeBras, G., MacLeod, H., and Teton, S.:
788 Rate constants for the reactions of hydroxyl radicals and chlorine atoms with halogenated aldehydes, J. Phys. Chem., 97, 4683-
789 4688, https://doi.org/10.1021/j100120a021, 1993.

790 Sellevåg, S. R., Stenstrøm, Y., Helgaker, T., and Nielsen, C. J.: Atmospheric Chemistry of CHF_2CHO: Study of the IR and
791 UV−Vis Absorption Cross Sections, Photolysis, and OH-, Cl-, and NO3-Initiated Oxidation, J. Phys. Chem. A, 109, 3652-
792 3662, https://doi.org/10.1021/jp050313m, 2005.

793 Sivakumaran, V., Hölscher, D., Dillon, T. J., and Crowley, J. N.: Reaction between OH and HCHO: temperature dependent
794 rate coefficients (202–399 K) and product pathways (298 K), Phys. Chem. Chem. Phys., 5, 4821-4827,
795 https://doi.org/10.1039/B306859E, 2003.

796 Stone, D., Whalley, L. K., and Heard, D. E.: Tropospheric OH and HO_2 radicals: field measurements and model comparisons,
797 Chem. Soc. Rev., 41, 6348-6404, https://doi.org/10.1039/C2CS35140D, 2012.

798 Stone, D., Blitz, M., Daubney, L., Howes, N. U. M., and Seakins, P.: Kinetics of CH_2OO reactions with SO_2, NO_2, NO, H_2O
799 and CH_3CHO as a function of pressure, Phys. Chem. Chem. Phys., 16, 1139-1149, https://doi.org/10.1039/C3CP54391A, 2014.

800 Sun, Y., Long, B., and Truhlar, D. G.: Unimolecular Reactions of E-Glycolaldehyde Oxide and Its Reactions with One and
801 Two Water Molecules, Research, 6, 0143, https://doi.org/10.34133/research.0143, 2024.

802 Taatjes, C. A., Welz, O., Eskola, A. J., Savee, J. D., Osborn, D. L., Lee, E. P. F., Dyke, J. M., Mok, D. W. K., Shallcross, D. E.,
803 and Percival, C. J.: Direct measurement of Criegee intermediate (CH_2OO) reactions with acetone, acetaldehyde, and
804 hexafluoroacetone, Phys. Chem. Chem. Phys., 14, 10391-10400, https://doi.org/10.1039/C2CP40294G, 2012.

805 Tereszchuk, K. A. and Bernath, P. F.: Infrared absorption cross-sections for acetaldehyde (CH_3CHO) in the 3μm region, J.
806 Quant. Spectrosc. Radiat. Transfer, 112, 990-993, https://doi.org/10.1016/j.jqsrt.2010.12.003, 2011.

807 Thévenet, R., Mellouki, A., and Le Bras, G.: Kinetics of OH and Cl reactions with a series of aldehydes, Int. J. Chem. Kinet.,
808 32, 676-685, https://doi.org/10.1002/1097-4601(2000)32:11<676::AID-KIN3>3.0.CO;2-V, 2000.

809 Wang, P.-B., Truhlar, D. G., Xia, Y., and Long, B.: Temperature-dependent kinetics of the atmospheric reaction between
810 CH2OO and acetone, Phys. Chem. Chem. Phys., 24, 13066-13073, https://doi.org/10.1039/D2CP01118B, 2022.

811 Wei, Y., Zhang, Q., Huo, X., Wang, W., and Wang, Q.: The reaction of Criegee intermediates with formamide and its
812 implication to atmospheric aerosols, Chemosphere, 296, 133717, https://doi.org/10.1016/j.chemosphere.2022.133717, 2022.

813 Wenger, J. C.: Chamber Studies on the Photolysis of Aldehydes Environmental, Environmental Simulation Chambers:
814 Application to Atmospheric Chemical Processes, Dordrecht, pp, 111-119, 2006.

815 Werner, H.-J., Knowles, P. J., Knizia, G., Manby, F. R., Schütz, M., Celani, P., Györffy, W., Kats, D., Korona, T., Lindh, R.,
816 Mitrushenkov, A., Rauhut, G., Shamasundar, K. R., Adler, T. B., Amos, R. D., Bennie, S. J., Bernhardsson, A., Berning, A.,
817 Cooper, D. L., Deegan, M. J. O., Dobbyn, A. J., Eckert, F., Goll, E., Hampel, C., Hesselmann, A., Hetzer, G., Hrenar, T., Jansen,
818 G., Köppl, C., Lee, S. J. R., Liu, Y., Lloyd, A. W., Ma, Q., Mata, R. A., May, A. J., McNicholas, S. J., Meyer, W., Miller III, T.
819 F., Mura, M. E., Nicklass, A., O'Neill, D. P., Palmieri, P., Peng, D., Pflüger, K., Pitzer, R., Reiher, M., Shiozaki, T., Stoll, H.,
820 Stone, A. J., Tarroni, R., Thorsteinsson, T., Wang, M., and Welborn, M.: MOLPRO, version 2019.2, a package of ab initio
821 programs, https://www.molpro.net/ (last access: 17 October 2025), 2019.

822 Xia, Y., Long, B., Liu, A., and Truhlar, D. G.: Reactions with Criegee intermediates are the dominant gas-phase sink for formyl
823 fluoride in the atmosphere, Fundam. Res., 4, 1216-1224, https://doi.org/10.1016/j.fmre.2023.02.012, 2024.

824 Xia, Y., Zhang, W., Tang, X., and Long, B.: Quantitative Kinetics of the Hydrogen Shift Reaction of Methylthiomethyl Peroxy
825 Radical (CH_3SCH_2OO) in the Atmosphere, J. Phys. Chem. A, 129, 2275-2285, https://doi.org/10.1021/acs.jpca.4c06818, 2025.

826 Xia, Y., Long, B., Lin, S., Teng, C., Bao, J. L., and Truhlar, D. G.: Large Pressure Effects Caused by Internal Rotation in the
827 s-cis-syn-Acrolein Stabilized Criegee Intermediate at Tropospheric Temperature and Pressure, J. Am. Chem. Soc., 144, 4828-
828 4838, https://doi.org/10.1021/jacs.1c12324, 2022.

829 Yang, X., Xue, L., Wang, T., Wang, X., Gao, J., Lee, S., Blake, D. R., Chai, F., and Wang, W.: Observations and Explicit
830 Modeling of Summertime Carbonyl Formation in Beijing: Identification of Key Precursor Species and Their Impact on
831 Atmospheric Oxidation Chemistry, J. Geophys. Res.: Atmos., 123, 1426-1440, https://doi.org/10.1002/2017JD027403, 2018.

832 Zhang, L., Truhlar, D. G., and Sun, S.: Association of Cl with C2H2 by unified variable-reaction-coordinate and reaction-path
833 variational transition-state theory, Proc. Natl Acad. Sci., 117, 5610-5616, https://doi.org/10.1073/pnas.1920018117, 2020.

834 Zhang, R. M., Xu, X., and Truhlar, D. G.: TUMME: Tsinghua University Minnesota Master Equation program, Comput. Phys.
835 Commun., 270, 108140, https://doi.org/10.1016/j.cpc.2021.108140, 2022.

836 Zhang, T., Wen, M., Ding, C., Zhang, Y., Ma, X., Wang, Z., Lily, M., Liu, J., and Wang, R.: Multiple evaluations of atmospheric
837 behavior between Criegee intermediates and HCHO: Gas-phase and air-water interface reaction, J. Environ. Sci., 127, 308-
838 319, https://doi.org/10.1016/j.jes.2022.06.004, 2023.

839 Zhang, Y., Mu, Y., Liu, J., and Mellouki, A.: Levels, sources and health risks of carbonyls and BTEX in the ambient air of
840 Beijing, China, J. Environ. Sci., 24, 124-130, https://doi.org/10.1016/S1001-0742(11)60735-3, 2012.

841 Zhao, M., Shen, H., Zhang, J., Liu, Y., Sun, Y., Wang, X., Dong, C., Zhu, Y., Li, H., Shan, Y., Mu, J., Zhong, X., Tang, J., Guo,
842 M., Wang, W., and Xue, L.: Carbonyl Compounds Regulate Atmospheric Oxidation Capacity and Particulate Sulfur Chemistry
843 in the Coastal Atmosphere, Environ. Sci. Technol., 58, 17334-17343, https://doi.org/10.1021/acs.est.4c03947, 2024.

844 Zheng, J. and Truhlar, D. G.: Multi-path variational transition state theory for chemical reaction rates of complex polyatomic
845 species: ethanol + OH reactions, Faraday Discuss., 157, 59-88, https://doi.org/10.1039/C2FD20012K, 2012.

846 Zheng, J., Zhang, S., and Truhlar, D. G.: Density Functional Study of Methyl Radical Association Kinetics, J. Phys. Chem. A,
847 112, 11509-11513, https://doi.org/10.1021/jp806617m, 2008.

848 Zheng, J., Mielke, S. L., Clarkson, K. L., and Truhlar, D. G.: MSTor: A program for calculating partition functions, free energies,
849 enthalpies, entropies, and heat capacities of complex molecules including torsional anharmonicity, Comput. Phys. Commun.,
850 183, 1803-1812, https://doi.org/10.1016/j.cpc.2012.03.007, 2012.

851 Zheng, J., Bao, J. L., Meana-Pañeda, R., Zhang, S., J.Lynch, B., Corchado, J. C., Chuang, Y., Fast, P. L., Hu, W.-P., Liu, Y.-P.,
852 Lynch, G. C., Nguyen, K. A., Jackels, C. F., Ramos, A. F., Elling son, B. A., Melissas, V. S., Villà, J., Rossi, I., Coitiño, E. L.,
853 Pu, J., Albu, T. V., Ratkiewicz, A., Steckler, R., Garrett, B. C., Isaacson, A. D., and Truhlar, D. G.: Polyrate-version 2017-C;
854 University of Minnesota: Minneapolis, 2017.

855 Zheng, J., Bao, J. L., Zhang, S., Corchado, J. C., Chuang, Y., Ellingson, B. A., and Truhlar, D. G.: Gaussrate, version 2017-B;
856 University of Minnesota: Minneapolis, MN, https://comp.chem.umn.edu/polyrate/ (last access: 17 October 2025), 2018.

857 Zhu, L., Talukdar, R. K., Burkholder, J. B., and Ravishankara, A. R.: Rate coefficients for the OH + acetaldehyde (CH_3CHO)
858 reaction between 204 and 373 K, Int. J. Chem. Kinet., 40, 635-646, https://doi.org/10.1002/kin.20346, 2008.

859

860